

Zero-shot capability of SAM-family models for bone segmentation in CT scans

Caroline Magg^{1,2}, Hoel Kervadec^{1,2}, Clara I. Sánchez^{1,2}

¹ University of Amsterdam, The Netherlands

² Amsterdam UMC location University of Amsterdam, The Netherlands

Abstract

The Segment Anything Model (SAM) and similar models build a family of promptable foundation models (FMs) for image and video segmentation. The object of interest is identified using prompts, such as bounding boxes or points. With these FMs becoming part of medical image segmentation, extensive evaluation studies are required to assess their strengths and weaknesses in clinical setting. Since the performance is highly dependent on the chosen prompting strategy, it is important to investigate different prompting techniques to define optimal guidelines that ensure effective use in medical image segmentation. Currently, no dedicated evaluation studies exist specifically for bone segmentation in CT scans, leaving a gap in understanding the performance for this task. Thus, we use non-iterative, “optimal” prompting strategies composed of bounding box, points and combinations to test the zero-shot capability of SAM-family models for bone CT segmentation on three different skeletal regions. Our results show that the best settings depend on the model type and size, dataset characteristics and objective to optimize. Overall, SAM and SAM2 prompted with a bounding box in combination with the center point for all the components of an object yield the best results across all tested settings. As the results depend on multiple factors, we provide a guideline for informed decision-making in 2D prompting with non-interactive, “optimal” prompts.

Keywords Segment anything model, Medical image segmentation, Foundation models, Bone segmentation

1 Introduction

The release of Segment Anything Model (SAM) [10] started a family of promptable foundation models (FMs) for segmentation. Spatial or textual information in form of bounding box, points inside and outside the object or descriptive text are used as prompts to identify the object of interest. FMs are trained on huge datasets and their design allows them to generalize to unseen tasks and data. As data scarcity and domain shifts are common problems in medical image segmentation, FMs enter medical image segmentation as new alternative to fully supervised, specialized models trained on annotated data.

Since SAM and its extension SAM2 (for video segmentation) are trained on natural image materials, there remains a gap in application to medical data due to the domain shift (natural images vs. medical images) and modality differences (2D vs. 3D). Efforts to address this gap have focused on fine-tuning and modifying the SAM architecture to improve its suitability for medical imaging, resulting in versions such as *Med-SAM* [12], *SAM-Med2d* [2], *SAM-Med3d* [20], *Med-SAM2* [27]. Beyond model adaptations, thorough evaluation studies are essential to understand the current performance behavior, to identify potential weaknesses, risks and limitations in clinical settings and to formulate application guidelines for specific medical use cases.

Table 1 collects a selection of evaluation studies closely related to our work, especially those conducted with a variety of medical image datasets. The conclusion of several evaluation studies [1, 4, 6, 7, 13, 14] is the unstable performance across different datasets and task. The models tend to struggle with small, irregular structures with low-contrast or fuzzy boundaries, leading to unsatisfying results. In contrast, they show promising results on larger structures with clear, sharp boundaries. Given that bone appears in CT scans with high-intensity values and well-defined boundaries, we hypothesize that SAM-family models are well-suited to achieve promising results for this task. While we do not claim that the provided list in Table 1 is exhaustive, a gap in current evaluation studies is recognizable: There is no dedicated study focused on CT scans for bone segmentation. Existing studies primarily only evaluate the performance of SAM and SAM2 across general medical imaging tasks, which allows them to use publicly available datasets. In contrast, our study utilizes a private dataset because many fine-tuned SAM models have already been trained on public CT datasets with bone segmentation labels, which prevents a fair comparison. Fig. 1 provides a timeline overview of relevant publications (i.e., FMs and evaluation studies from Table 1).

Table 1: Overview of evaluation studies similar to our work. The prompting strategies marked with \dagger are applied for the largest and multiple disconnected components of one object. Unknown model sizes are denoted as N/A. The last column indicates whether CT scans with bone segmentation are included in the dataset. \times^* corresponds to testing on X-Rays of the hip [5].

Authors	Prompting strategies	Models	Dataset	Bone CT
Roy et al. [16]	<ul style="list-style-type: none"> • pos. random points • perturbed bounding box 	SAM (size N/A)	1 public	\times
He et al. [6]	<ul style="list-style-type: none"> • mass center • dilated bounding box 	SAM (size N/A)	12 public	\times
Mazurowski et al. [14]	<ul style="list-style-type: none"> • center\dagger • bounding box\dagger • simulated interactive 2D prompting 	SAM (size N/A)	19 public	\times^*
Huang et al. [7]	<ul style="list-style-type: none"> • center of mass/positive point • 5 pos. random points • 5 pos. and neg. points • bounding box • bounding box + 1 positive point 	SAM (all sizes)	53 public	\checkmark
Cheng et al. [1]	<ul style="list-style-type: none"> • bounding box • center point of bounding box 	SAM (size N/A)	12 public	\times
Mattjie et al. [13]	<ul style="list-style-type: none"> • center • (distributed) pos. random points • (perturbed) bounding box 	SAM (all sizes)	6 public	\times^*
Dong et al. [4]	<ul style="list-style-type: none"> • center\dagger • bounding box\dagger 	SAM2 (size N/A)	18 public	\times^*
Shen et al. [19]	<ul style="list-style-type: none"> • pos. and neg. points • bounding box 	SAM, SAM2, Med-SAM, SAM-Med2 (sizes N/A)	1 public	\times
Sengupta et al. [18]	<ul style="list-style-type: none"> • pos. random points • 1 pos. and 2 neg. points 	SAM & SAM2 (all sizes)	11 public	\times
Yu et al. [23]	<ul style="list-style-type: none"> • 1 point (undefined) • bounding box 	SAM & SAM2 (size N/A)	2 public	\times
Our study	<ul style="list-style-type: none"> • center\dagger • centroid\dagger • bounding box\dagger • pos random points\dagger • bounding box + center\dagger • bounding box + pos/neg. points\dagger • center + 1,5 neg. points\dagger • 1,5 pos. + neg. points\dagger 	SAM, SAM2, Med-SAM, SAM-Med2d (all sizes)	3 private	\checkmark

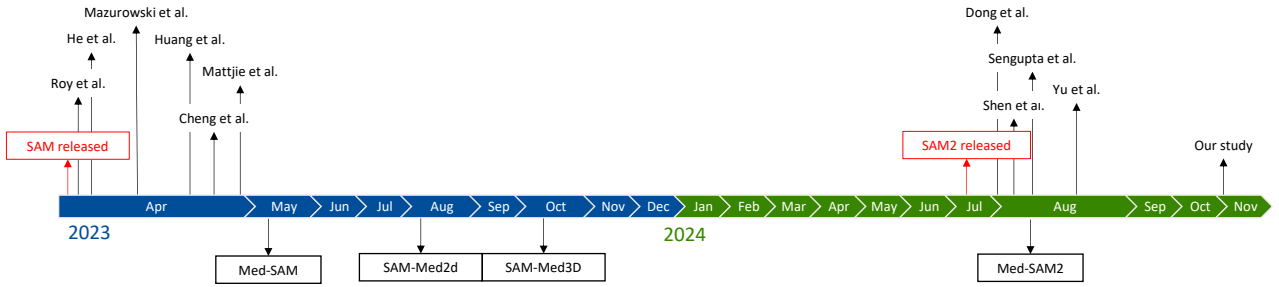


Figure 1: Timeline overview of relevant publications: models used for this study (highlighted with a bounding box) and related evaluation studies as mentioned in Table 1. The first timestamp of pre-prints (not accepted peer-reviewed publications) are used for the visualization.

As a first step, the aim of this study is to investigate different non-iterative prompting strategies for SAM-family models on bone segmentation in CT scans under “optimal” 2D settings, i.e., prompts are based on reference masks without manipulation or human error. We test 9 SAM-family models with 32 prompting strategies on three different skeletal regions containing different bone structures. Based on our extensive analysis considering segmentation performance and model inference time, we introduce a preliminary guideline for choosing a 2D prompting strategy and model for a use case.

2 SAM-family

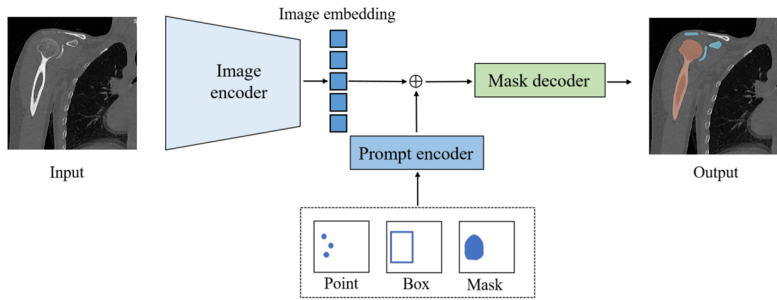
We refer to SAM and its related FMs as the SAM-family, each model used in our evaluation study described in the following section.

2.1 SAM

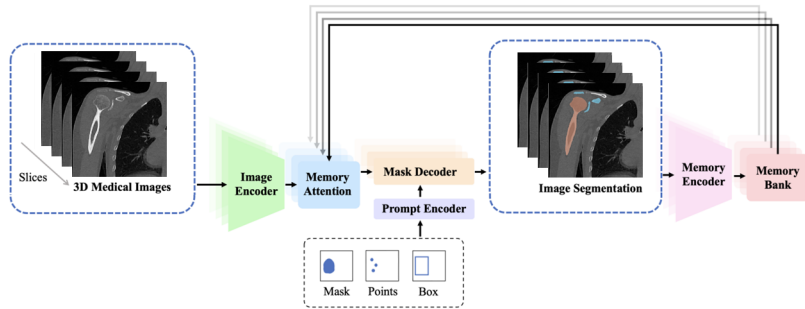
The Segment Anything Model (SAM) [10] was introduced in April 2023 by *Meta* as promptable “foundation model for image segmentation”. SAM supports sparse prompts, i.e., bounding box and clicks (positive and negative), and dense prompts, i.e., masks. The architecture consists of three parts (Fig. 2a): First, the image encoder, a Masked Autoencoder (MAE) pre-trained Vision Transformer (ViT), is run once per image to create image embeddings of the 2D image input. Then, the prompt encoder creates prompt embeddings, i.e., the sum of positional encodings and learned embeddings, for each prompt type. Finally, the lightweight mask decoder combines both embeddings and an output token and predicts the final segmentation mask. Since prompts can be ambiguous, the model produces by default three masks with confidence scores that are based on estimated IoU. We employ the option for a single output mask. The model was trained in three stages employing a model-assisted annotation workflow to annotate the final training dataset SA-1B, which consists of 11M images and over 1B masks. The model is available in three different sizes: base (B), huge (H) and large (L), which depends on the ViT encoder.

2.2 SAM2

SAM2 [15] was introduced in July 2024 as extension to SAM with the capability of image and video segmentation. This is realized by changes in the architecture (Fig. 2b): The ViT encoder is replaced by a MAE pre-trained Hiera image encoder, making use of multi-scale features. The image encoder is run once per interaction to produce unconditioned embeddings for each frame. The memory attention block fuses the unconditioned embeddings of a frame with past frame features and predictions. The conditioned embeddings are combined with new available prompt embeddings. Since not every frame



(a) SAM architecture with image & prompt encoder and mask decoder; Image adapted from [26].



(b) SAM2 architecture with image & prompt encoder, mask decoder and memory mechanics; Image adapted from [25].

Figure 2: Comparison of the SAM and SAM2 architectures.

in a video might contain the object of interest due to occlusion, the mask decoder is enhanced by an additional occlusion head to allow for an empty prediction. The generated segmentation masks are downsampled and combined with the unconditioned frame embedding to build a spatial feature map. This created memory is fed to a FIFO queue in the memory bank, where information of up to N recent frames and K prompted frames are stored. The model was trained on SA-V, the Segment Anything Video dataset with 35.5M masks in 50.9K videos, in multiple training iterations. Due to different Hieras sizes, four different SAM2 sizes are available: base plus (B+), tiny (T), small (S) and large (L).

2.3 Med-SAM

Ma et al. introduced *Med-SAM* [12] as “a foundation model for promptable medical image segmentation”. Without any adaptations to the SAM architecture, they fine-tuned SAM B on a medical image dataset. While keeping the prompt encoder frozen, all trainable parameters in the image encoder and the mask decoder are trained for 150 epochs. The training dataset with focus on cancer types contains more than one million image-mask pairs including 10 imaging modalities. *Med-SAM* was only retrained for bounding box prompts, as the authors argue that for that task point-based prompts introduce a more ambiguous spatial context than bounding boxes.

2.4 SAM-Med2d

Cheng et al. developed *SAM-Med2d* [2] by fine-tuning SAM B with an adapter technique. The frozen image encoder is equipped with learnable adapter layers which are updated together with the prompt encoder and the mask decoder during 9 training iterations with 12 epochs. The model keeps

the functionality of both sparse prompts (bounding box and point), while using also dense prompts (masks) during training. For fine-tuning, the dataset SA-Med2D-20M [22] was curated from public and private datasets, where 20M corresponds to the number of masks.

3 Dataset

As medical SAM versions (e.g., *Med-SAM* [12], *SAM-Med2D* [2], *SAM-Med3d* [20]) are fine-tuned on publicly available datasets containing bone segmentation on CT scans (i.e., TotalSegmentator [21], CTPelvic1K [11], VerSe2020 [17]), an independent dataset is required to ensure a fair comparison across all models. Thus, we compiled a private (from the department of Orthopedic Surgery and Sports Medicine of the Amsterdam UMC) dataset of 80 CT Scans with three different skeletal regions (Fig. 3):

- D1 Shoulder: 15 bilateral scans with 4 labels for left and right scapula and humerus.
- D2 Wrist: 40 unilateral scans with 6 labels for capitate, lunate, radius, scaphoid, triquetrum, and ulna.
- D3 Knee: 25 unilateral scans with 2 labels for tibia bone and tibia implant. There are two different labeling protocols for the tibia bone: cortical bone (D3a) and full bone (D3b).

All scans were acquired with a Brilliance 64-channel CT Scanner (Philips Healthcare, Best, The Netherlands) or a Siemens SOMATOM Force with 160 mAs, 120 kV. The isotropic voxel spacing is 0.93 mm, 0.32 mm, and 0.48 mm, for D1, D2, and D3, respectively. The annotations were generated using an in-house annotation software [3] and/or ITK-Snap [24].

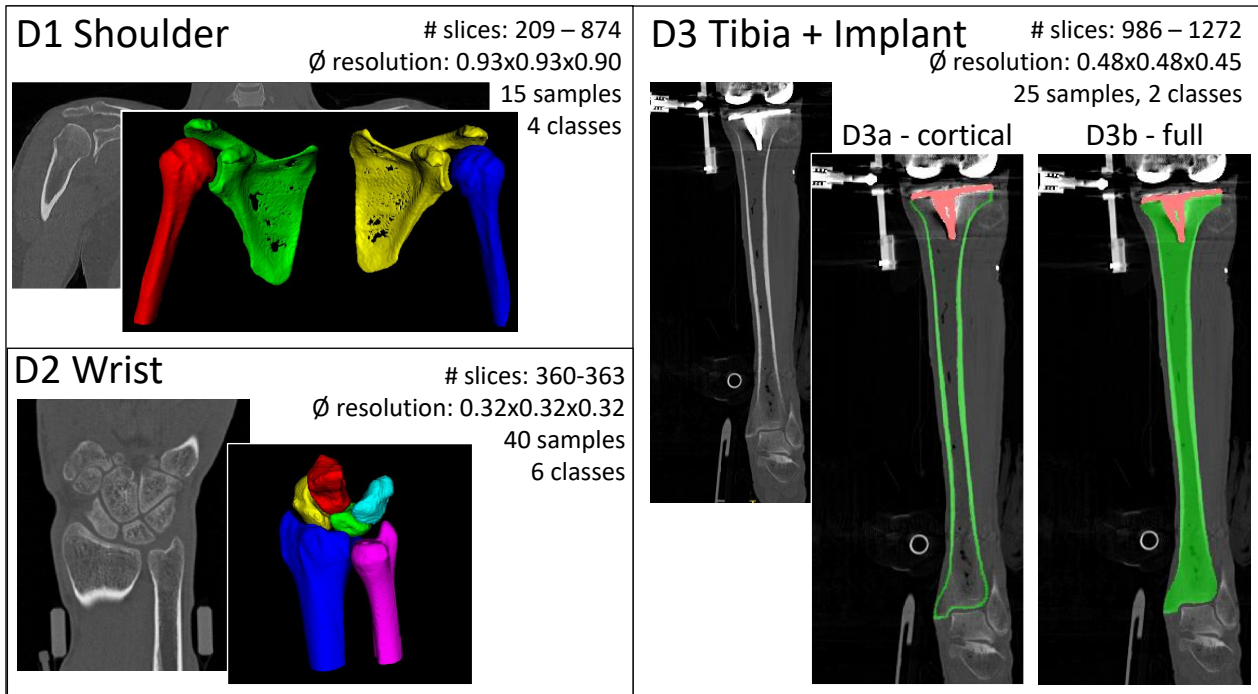


Figure 3: Dataset Overview: 3 private datasets containing 80 CT scans from three skeletal regions, i.e., shoulder (D1), wrist (D2) and knee (D3) are used. The knee dataset comes with two different sets for the tibia segmentation, i.e., cortical (D3a) and full (D3b) tibia segmentation.

4 Experimental Setup

4.1 Prompting Strategies

We use non-iterative prompts, which are automatically extracted from the reference masks. A prompt consists of at least one prompt primitive (i.e., **bounding box**, **center**, **centroid**, **positive**, **negative** points) and one component selection criteria (i.e., largest (1C) or up to 5 components (5C)).

4.1.1 Primitives

There are 5 primitives which are the building blocks for a prompt (Fig. 4):

- (a) **bounding box**: Enclosing tight rectangle, i.e., no extra space between the object boundary and the box.
- (b) **(EDT) center**: Maximum location of the Euclidean distance transform (EDT), i.e., the point the most further away from the object boundary. In case of equality (two points or more are as far as possible from the boundary), a random point is selected. For shortness, we refer to it simply as **center** from now on.
- (c) **centroid**: Center of mass with homogeneous density. Note that there is no guarantee that the centroid is inside the object. Despite this shortcoming, we include it as other existing work [6] used it.
- (d) **positive points**: Random points within the region. To avoid random points on the border, the reference mask is eroded by a 3×3 ellipsoidal kernel before the random points are extracted.
- (e) **negative points**: Random points outside the region close to the border. To ensure that the points remain near the object and prevent scattering across distant image regions, a margin through mask dilation is created for point extraction. The mask is dilated in two steps: first the mask is dilated with a 5×5 ellipsoidal kernel and then with a 15×15 ellipsoidal kernel. The difference between these two dilated regions is used for point extraction.

The prompt primitives are extracted for each component of the reference mask larger than 15 pixels or larger than 5% of the entire component in a slice. Fig. 5 illustrates that components that are smaller as the defined criteria are unrealistic to be annotated: bounding boxes are collapsing and there are not enough pixels to extract 10 random points inside the object. The thresholds were chosen empirically after dataset inspection.

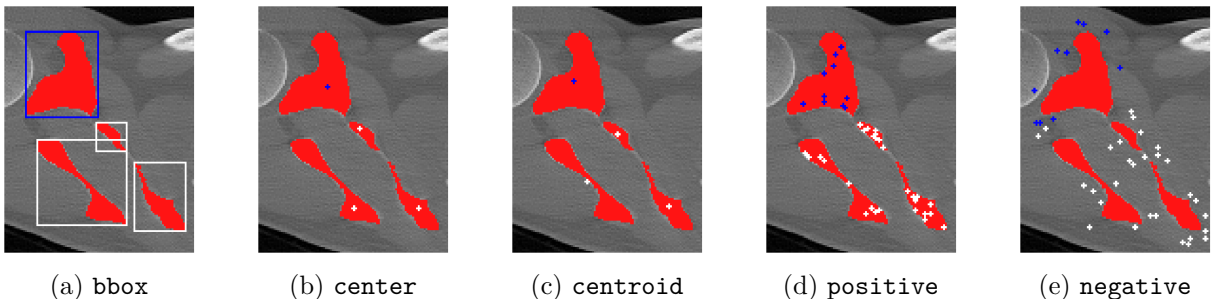


Figure 4: Prompt primitives: (a) bounding box, (b) (EDT) center, (c) centroid, (d) positive random points inside the object, (e) negative random points outside the object. The largest component’s prompt is blue (i.e., one component (1C)), while the others are white, resulting in the setting with up to 5 components (5C), when all prompts are used.

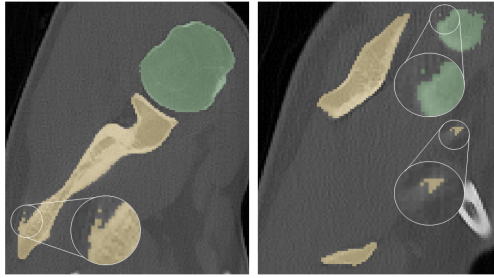


Figure 5: Examples for small components in reference masks that are ignored during prompt primitive extraction. The zoomed-in windows show small reference masks that do not meet the criteria of being at least 15 pixels in size or covering more than 5% of the total component in the slice.

4.1.2 Component selection criteria

As shown in Fig. 4, anatomical structures can consist of multiple disconnected components in a 2D medical image slice. In our datasets, the number of disconnected components does not exceed 6, which only occurs for less than 10 slices in our entire dataset. Thus, for a prompt, the primitives of either the largest component (1C, denoted as open symbols) or up to 5 components (5C, denoted as closed symbols) are used. As those foundational models claim to perform very well in zero-shot scenarios, we expect them to generalize well to the other connected components, even if they are not directly selected with a point or bounding box.

4.1.3 2D Prompts

A 2D prompting strategy is defined by one or more prompt primitives and one component selection criteria. 2D strategies can be divided into three categories based on the involved primitives:

- One-type prompts (OT prompts): bounding box (\square), center (\odot), centroid (\circ), 1, 3, 5 or 10 positive random points (\triangle , \triangleright , ∇ , \triangleleft).
- bounding box + point combination prompts (BPC prompts): bounding box with center (\blacksquare), with 1 or 5 positive random points (\boxplus , \boxtimes), with 1 or 5 negative random points (\boxminus , \boxdiv).
- Point based combination prompts (PB prompts): center with 1 or 5 negative points (\blacktriangle , \blacktriangledown), 1 or 5 positive and negative random points (\blacktriangle , \blacktriangledown).

Certain redundant combinations have been omitted to reduce the number of prompting strategies: The centroid is an unreliable primitive since it may lie outside the object depending on the object’s shape, so it is not used for combinations. Combinations with random points are done with one point as comparison to the center point and with five points to asses the effect of an increased number of points. In total, there are 32 settings per model. An exception is *Med-SAM* with 2 settings, as the model only supports bounding boxes.

4.2 Implementation details

The official github repositories (i.e., *SAM*¹, *SAM2*², *Med-SAM*³, *SAM-Med2d*⁴) are used for all models. Data preprocessing and weight download is performed as instructed. For *SAM2*, the weights from

¹<https://github.com/facebookresearch/segment-anything>, commit 6fdee8f

²<https://github.com/facebookresearch/sam2>, commits 0e78a11 & 29267c8

³<https://github.com/bowang-lab/MedSAM>, commit 2b7c64c

⁴<https://github.com/OpenGVLab/SAM-Med2D>, commit bfd2b93

July 29, 2024 are used. The evaluation is performed on GPUs NVIDIA Geforce RTX 2080 Ti 12GB and an Intel Core Xeon Gold 6128 3.40GHz CPU, which are embedded in a server accessible to multiple users. Evaluation code is adapted from [8, 9]. Visualizations are performed with 3D Slicer (<https://www.slicer.org/>) and plotly (<https://plotly.com/>).

4.3 Evaluation

Two common segmentation performance metrics, i.e., Dice Similarity Coefficient (DSC) and 95%-percentile Hausdorff Distance (HD95), were used to compare all prediction masks with the reference labels. In addition to performance metrics, the inference time for each model prediction was measured. The inference time includes the recommended image and prompt preprocessing and each prediction call, but excludes image and prompt loading. For models with multiple prediction calls due to multi-class segmentation (i.e., each class requires a separate prediction call as binary segmentation masks are returned), the image embedding is done once and reused for all class predictions.

To compare FMs with fully supervised models, 2D and 3D full resolution nnUNets [8] were trained for each subset. The training details are reported in Appendix A. The results are denoted as \star .

5 Results

5.1 Segmentation performances

5.1.1 Overview

Considering pure performance metrics (i.e., maximizing DSC or HD95 or both), the bottom right corner of Fig. 6 shows an overview of all methods with high DSC and low HD95 averaged over all datasets. *SAM B* with bounding box + center 5C (■) has the highest DSC of 92.5% (1.7 mm HD95), whereas *SAM L* with bounding box + center 1C (◻) has the lowest HD95 with 1.1 mm (92.1% DSC). 59 out of 258 methods achieve a DSC higher than 91%: 28 *SAM* and 31 *SAM2* methods; 43 methods achieve a HD95 lower than 2 mm: 23 *SAM* and 20 *SAM2* methods. The five highest DSC values (> 92%) are achieved by *SAM* methods. A similar visualization for each dataset individually can be found in Appendix C.1, Fig. 20. The highest DSC reached *SAM H* with center + 5 negative points 5C for D1 (92.8%), *SAM2 L* with bounding box + 5 positive points 1C for D2 (97.2%), *SAM2 B* with bounding box + 5 negative points 1C for D3a (77.3%), and *SAM B* with bounding box + center 1C for D3b (92.2%). The lowest HD95 have *SAM H* with bounding box + center 5C for D1 (1.0 mm), *SAM2 T* with bounding box + center 5C for D2 (0.4 mm), *SAM L* with bounding box 5C for D3a (2.7 mm), and *SAM B* with bounding box + center 1C for D3b (1.9 mm). Visual examples are shown in Fig. 7, and Appendix B.3, Fig. 15 - 19.

5.1.2 Best performing prompts

Fig. 8 shows the 10 best performing 2D prompting strategies across different models: bounding box 5C and 1C, bounding box + center 5C and 1C, bounding box + 1 positive point 5C and 1C, bounding box + 5 positive points 1C, bounding box + 1 negative points 5C and 1C, and bounding box + 5 negative points 5C (■, □, ●, ◻, ⊕, ⊞, ⊗, ⊘, ◆, ◇). They are determined by ranking the prompts from 1 to 32 (1 being the best) for each model based on their average DSC over all datasets. For the top 10 strategies, *SAM H* has the highest DSC with 91.6% and the lowest HD95 with 1.73 mm, followed by *SAM L* and *SAM B* with DSC around 91% and HD95 between 1.8 and 2.5 mm. *SAM2* models achieve DSC around 90% and HD95 of 2.8, 3.7, 5.2 and 7.4 mm for *SAM2 L, S, T, B+*, respectively. *SAM-Med2d* has 82.3% DSC and 4.3 mm HD95. *Med-SAM* has 75.3% DSC and 3.9 mm HD95. As an example for a fully supervised model, the performance of the individually dedicated nnUNets is averaged: 97.7% DSC and 1.7 mm HD95 for 3D full resolution

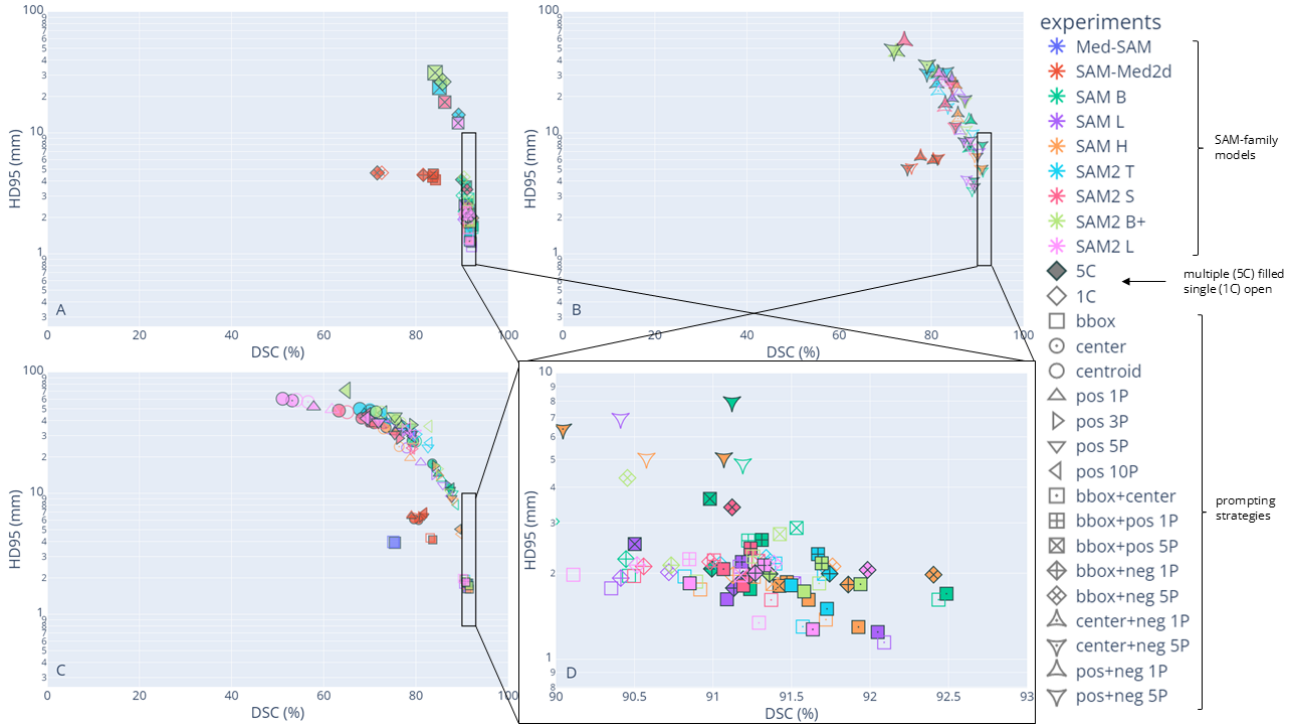


Figure 6: Performance of 2D prompting strategies: Scatterplots of BPC prompts (A), PC prompts (B), OT prompts (C) and zoomed-in view to the lower right corner (D). The symbol size in (A)-(C) is determined by the DSC standard deviation (std), i.e., bigger symbol means higher DSC std. The lower right corner, i.e., high DSC and low HD95 metrics, contains the performance strongest settings.

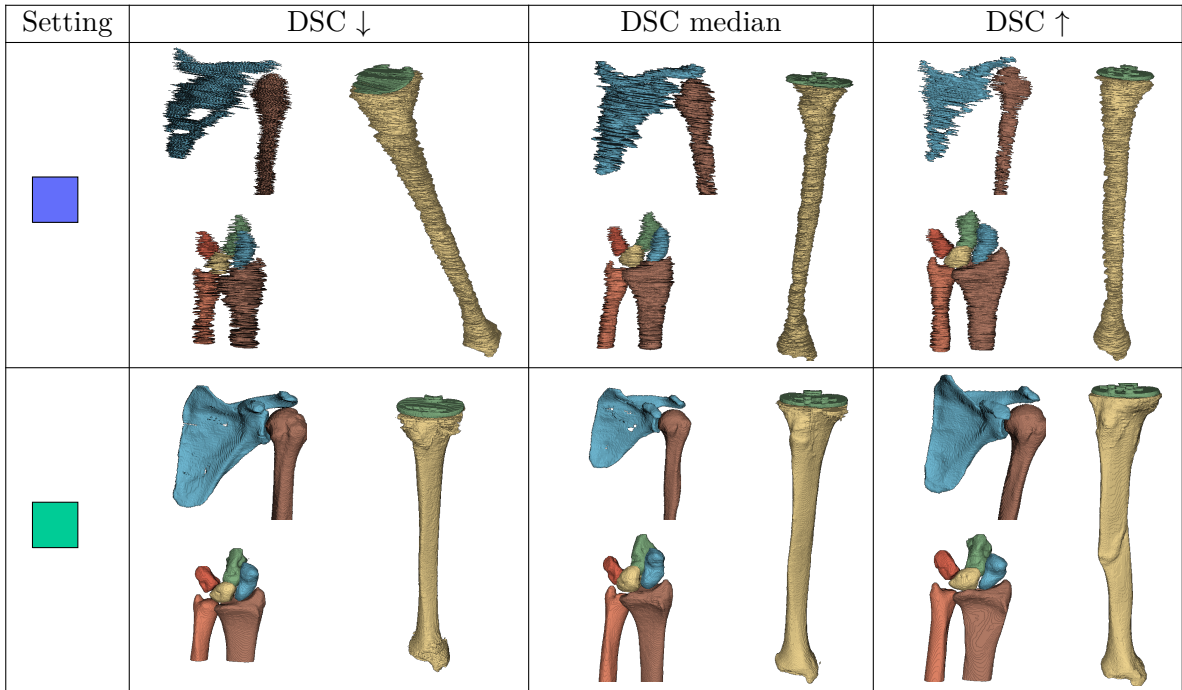


Figure 7: Selected visual examples for bounding box 5C for *Med-SAM*  and *SAM B*  with low, medium and high DSC (%).

nnUNet; 97.9% DSC and 4.1 mm HD95 for 2D nnUNet.

A similar ranking for each dataset individually is reported in Appendix D, Table 3. New strategies in the top 10 are center + 5 negative points 1C for D1, 5 positive + negative points 1C for D2, bounding box + 5 positive points 1C and bounding box + 5 negative points 1C for D3a, bounding box + 5 positive points 1C and 5 positive + negative points 1C for D3b.

Prompt	avg Ranking	DSC (%) avg (std)	HD95 (%) avg (std)
■	2.38	90.89 (10.0)	1.87 (2.7)
□	2.88	90.80 (10.0)	1.79 (2.1)
⊗	4.38	90.49 (10.2)	2.50 (2.8)
⊕	4.50	90.44 (9.6)	2.50 (2.6)
■	5.33	88.68 (10.4)	2.25 (2.2)
◆	6.25	90.15 (9.0)	2.26 (2.3)
⊞	7.38	90.22 (9.7)	2.49 (2.4)
□	9.67	88.03 (10.7)	2.39 (2.2)
◆	10.38	87.91 (10.2)	7.32 (16.1)
⊗	10.75	87.67 (14.1)	12.20 (28.1)

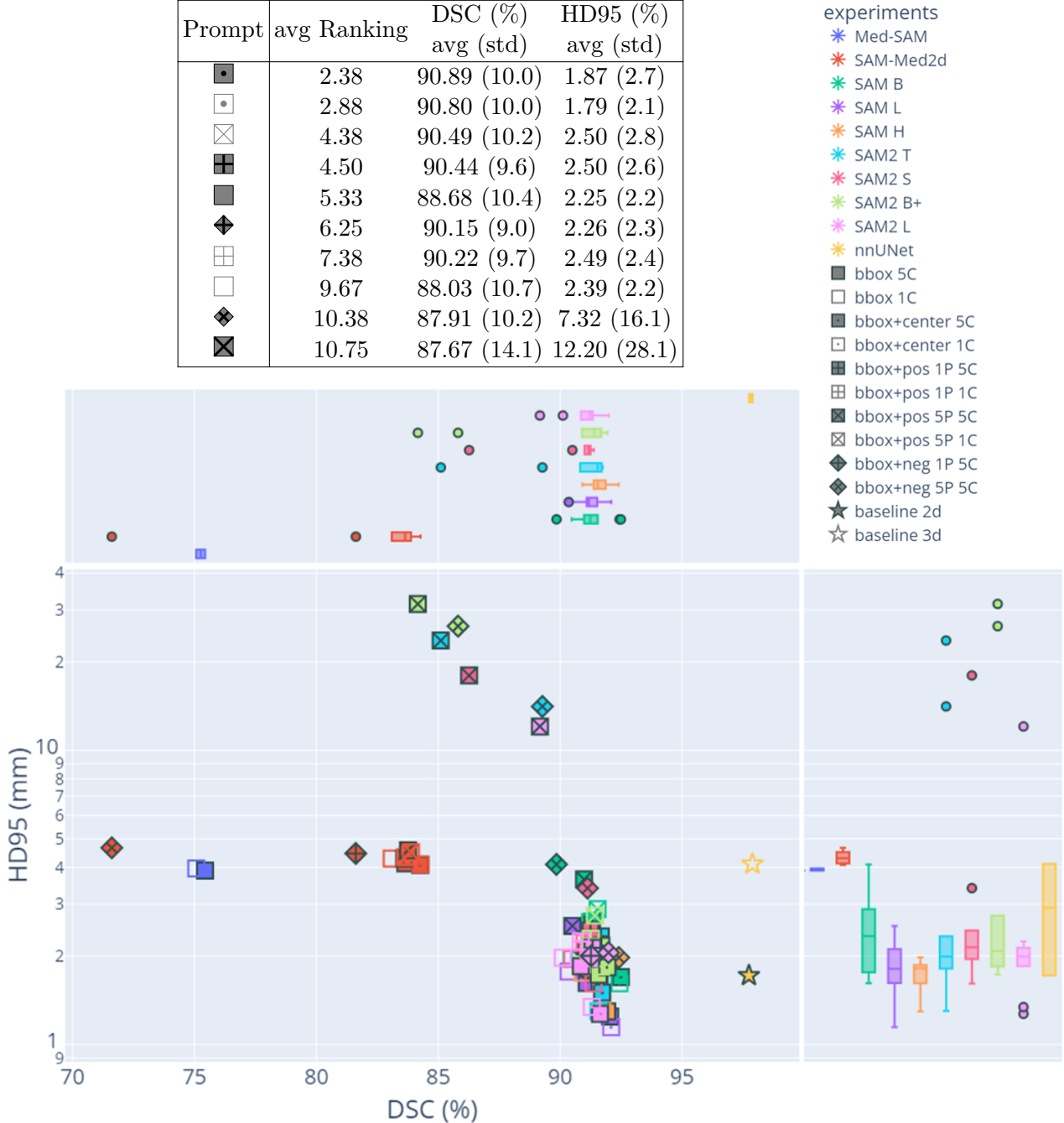
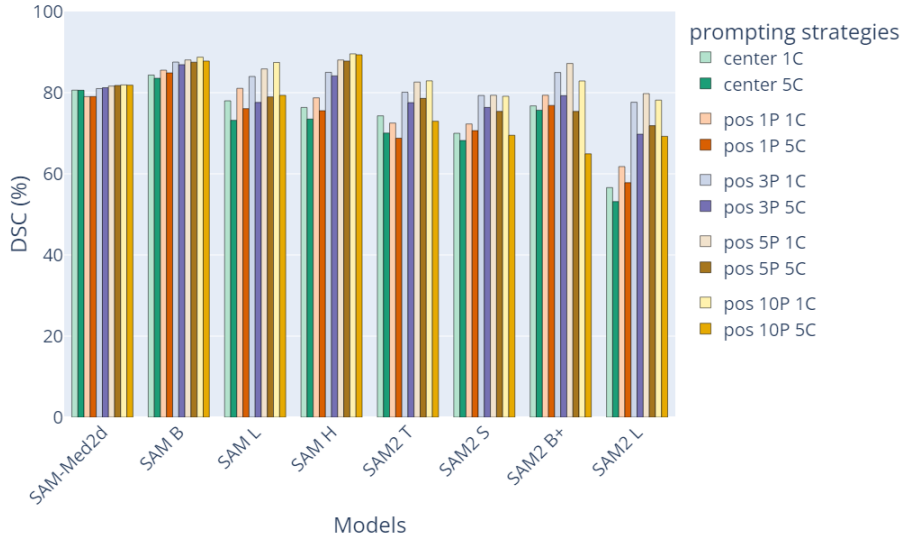


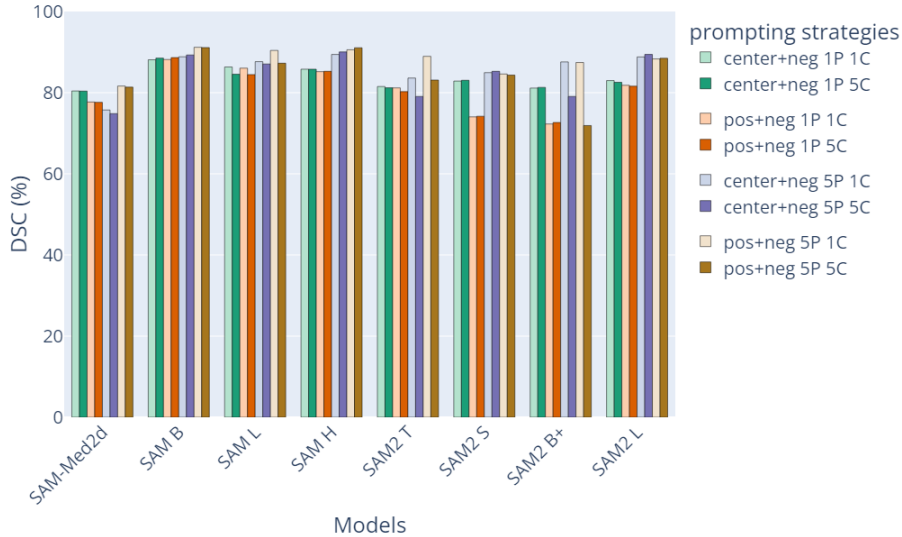
Figure 8: 10 best performing 2D prompting strategies across models: The prompt ranking is determined per model by means of the average DSC over all datasets (i.e., highest DSC corresponds to rank 1) and then averaged over all models. The visualization shows the scatter plot with the performance distribution per model across different prompting strategies. Note that the 10 best performing prompts are a subset of the prompts visualized in Fig. 6 D.

5.1.3 Different number of points

In Fig. 9 prompting strategies with different number of points are compared. For the point prompts, the best DSC achieves *SAM H 10 random points 1C* with 89.6%, followed by *SAM L 10 random points 1C* with 87.4% and *SAM2 B+ 5 random points 1C* with 87.2%. For *SAM-Med2d* and *SAM2 T* the best setting is 10 random points 1C, same as for all *SAM* models. The remaining *SAM2* models perform best with 5 random points 1C. For the point combination prompts, 5 positive + negative points performs best for *SAM H (5C, 91.1%)*, *SAM B (1C, 91.2%)* and *SAM L (1C, 90%)*. It is also the best setting for *SAM-Med2d* and *SAM2 T*. The remaining *SAM2* models work best with center + 5 negative points. The visualizations for each dataset individually are shown in Appendix C.2, Fig. 21. Visual examples are shown in Appendix B.2, Fig. 14.



(a) Center and positive random points



(b) Point combinations

Figure 9: DSC (%) performance for different number of points per model: (a) center point and 1,3,5,10 random positive points; (b) point combinations of center, 1 or 5 positive and negative points.

5.1.4 Different labeling protocols

For both subsets of the knee dataset (D3), the highest DSC is achieved with *SAM B* with **bounding box 5C** (74.2% DSC and 2.7 mm HD95) for D3a and with **bounding box + center 1C** (92.2% DSC and 1.9 mm HD95) for D3b. Fig. 10 shows the performance of both subsets for *SAM B* with all 2D prompting strategies. The full bone labeling protocol achieves higher DSC and lower HD95 for each prompting strategy. Visual examples are shown in Appendix B.1, Fig. 12.

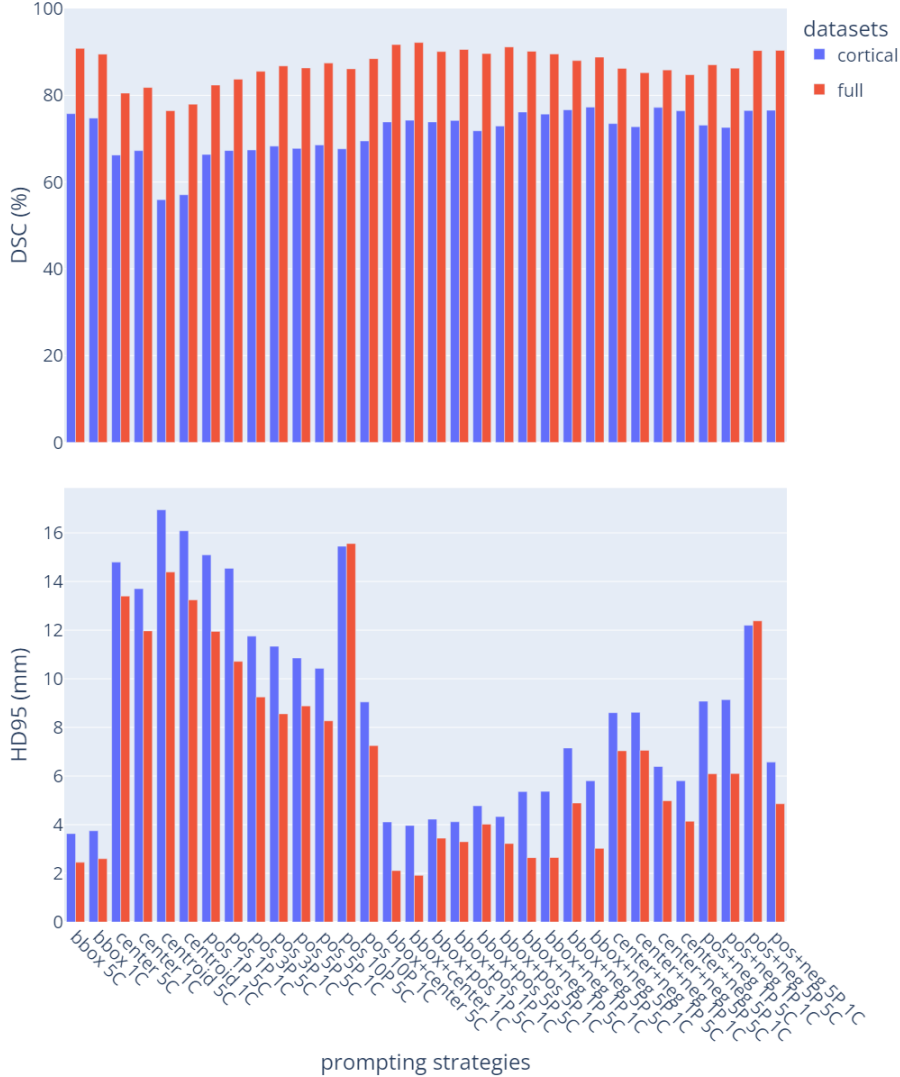


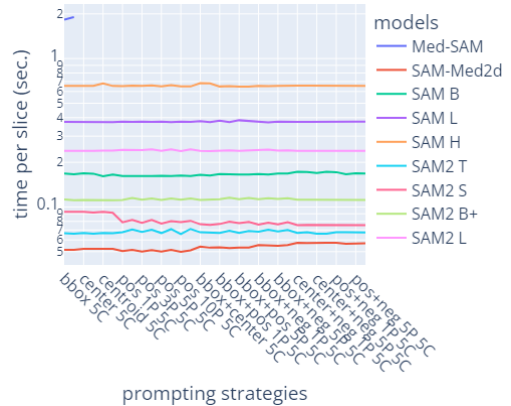
Figure 10: *SAM B* performance (top - DSC (%); bottom - HD95 (mm)) for different labeling protocols in the knee dataset (D3), i.e., cortical tibia bone (D3a) and full tibia bone (D3b).

5.2 Inference Time

As inference time per slice (sec.) might be related to number of model parameters, image sizes and prompting strategies, they are all reported together in Table 2. The fastest prediction time has *SAM-Med2D* with 0.052 sec per slice, followed by *SAM2* and *SAM* versions.

Table 2: Average prediction time per slice (sec.): The table on the left sorts the inference time averaged over all prompting strategies in ascending order. The line plot on the right shows the time per slice (sec.) for the different prompting strategies for each model.

Model	Avg. time per slice (s)	# Model Parameter	Image Size
SAM-Med2d	0.052	271	256x256
SAM2 T	0.068	38	1024x1024
SAM2 S	0.087	46	1024x1024
SAM2 B+	0.107	80	1024x1024
SAM B	0.150	93	1024x1024
SAM2 L	0.218	224	1024x1024
SAM L	0.332	312	1024x1024
SAM H	0.588	641	1024x1024
Med-SAM	1.658	93	1024x1024



6 Discussion

6.1 Segmentation performance

6.1.1 Overview

Med-SAM and *SAM-Med2d*, which are both fine-tuned on a medical image dataset containing CT scans, are outperformed by *SAM* and *SAM2*, trained on natural images, with most of the **bbox** based prompts. We attribute this to the unlearning of general representations caused by fine-tuning on a large variety of medical domains.

Fig. 6 shows a cluster of red symbols in (A)-(C) corresponding to the *SAM-Med2d* experiments. All prompt strategies have the same magnitude of HD95 (4-7 mm) and DSC between 71 % and 85 %. We conclude that the prompting strategy has little impact on the performance of *SAM-Med2d*. This is in contrast to *SAM* and *SAM2* experiments. The associated symbols form an arc from high DSC and low HD95 (“good” performance, i.e., lower right corner) to low DSC and high HD95 (“bad” performance, i.e., upper left quadrant) with increasing DSC standard deviation (i.e., increasing symbol size). The absence of obvious color and symbol clusters in the described arc shows that the performance is highly dependent on the prompting strategy and no overall best strategy can be determined. However, the zoomed-in lower right corner in Fig. 6 (D) shows three groups of prompting strategies: bounding box-only prompts and bounding box + point combinations in the lower half and point-based combination with 5 random points (i.e., center + 5 negative points and 5 positive + negative points) in the upper left quadrant.

6.1.2 Best performing prompts

The top 10 best performing prompting strategies across models with respect to DSC are bounding box-based, i.e., either bounding on its own or combined with point prompts (Fig. 8). For each dataset, the majority of the overall 10 best performing prompting strategies can also be found in the individual top 10, although the ranking position differs (Fig. 20, Table 3).

A comparison between FMs – such as *SAM*-based models – and nnUNet – a fully supervised and dedicated trained model – is not completely fair, as FMs do not have any prior knowledge about specific examples and nnUNet is explicitly trained for the given task. However, it gives us valuable insight about the capability and competitiveness of *SAM*-family models with current, established state-of-art-methods. Both nnUNet versions achieve a higher DSC. However, some *SAM*-based experiments

achieve a lower HD95, especially for the knee dataset (Table 3). This is due to the oversegmentation of the femur as tibia for nnUNet models (Fig. 13).

6.1.3 Different number of points

Comparing prompt strategies with different number of points shows that more points are not always better (Fig. 9). For *SAM-Med2D*, *SAM2 T* and *SAM* models, more random points result in better DSC, whereas for *SAM2* models five positive points achieve the highest DSC (Fig. 9a). Except for *SAM-Med2d* and *SAM2 T*, using the center point does not work better than one random positive point. Considering human-created annotations, this is promising: a human annotator may not place the point precisely at the center due to intensity differences in the object, and even when aiming for the center, the prompt might be slightly offset, resembling a random point placement inside the object. Comparing the point combinations shows that prompts with the center point perform better than the random point combination if there is only one positive point for *SAM2*, while with five positive points, the random point combinations demonstrates stronger performance for *SAM* (Fig. 9b). For all models, more negative points are better. We conclude that *SAM2* versions (except *SAM2 T*) do not need as many prompts as *SAM* to reach their best performance. However, while *SAM* models achieve their highest DSC with more points, also the DSC with the lower point equivalent is higher.

For some models, such as *SAM L* and *SAM2* models, there is a noticeable difference between the two component selection criteria, where taking the prompt from the largest component (1C) performs better than taking prompts from up to 5 components (5C). The latter results in oversegmentation of other bone structures (Fig. 14). This observations is particularly obvious for D1 (Fig. 21a), a dataset that contains an object (i.e., scapula) that is split into multiple components in axial slices.

6.1.4 Different labeling protocols

For the knee subset (D3), there are two different label sets available for the tibia bone, i.e., the cortical part of the bone (D3a) or the full bone (D3b). Independent of the prompting strategy, the cortical subset performs worse (Fig. 10). Inspecting visual examples reveals that despite prompt extraction from the cortical bone, the prediction frequently includes the whole bone (Fig. 12). We hypothesize that the prompts – both bounding box and point prompts – may be too ambiguous for the SAM-family models, leading the models to default to segmenting the full bone rather than individual components. Our objective in this work was to test generic prompting strategies without relying on dataset or task specific knowledge. However, to improve the segmentation of cortical bone, incorporating prior knowledge of the dataset and task could help mitigate ambiguities in the prompts. For example, consistently adding negative points in the center of the bone might guide the models more effectively towards the intended cortical bone structure. In future work, we intend to look further into the knee dataset to test this hypothesis and refine the prompting strategies on this specific task.

6.2 Inference time

As the evaluation was performed on a server that is available for multiple users, different server utilization can influence the exact inference time. Despite this limitation, a clear trend can be observed across different datasets, which were performed in separate evaluation runs. The inference time is highly influenced by the number of model parameters but not by the different prompting strategies (Table 2). The exceptions are the medically fine-tuned SAM-version. *Med-SAM* has the slowest inference time, which we attribute to code inefficiency, as the number of parameters and image size match with *SAM B*. *SAM-Med2d* has the fastest average inference time due to the smaller image size, as it is the only model using 256×256 . For all *SAM* and *SAM2* versions, the model size determines the inference time, i.e., the more model parameter, the longer the inference time.

6.3 Overall performance

6.3.1 Model sizes

Taking both segmentation performance and inference time into consideration, large models such as *SAM H* and *SAM L* are less favorable due to their longer average time per slice and *Med-SAM* and *SAM-Med2d* due to their sub-par performance. *SAM B* (*SAM* default model size), *SAM2 T* and *SAM2 B+* (*SAM2* default model size) provide a good trade-off between performance and runtime.

6.3.2 Prompting Strategies

Since the inference time is independent of the number of prompts, the general observations in Section 6.1 remain valid without the need for reconsideration:

- The overall best performing prompt is `bbox + center`.
- All top prompts across different models and datasets are bounding box-based: either bounding box-only or bounding box + point combinations.
- The best point combinations are `center + 5 negative points` for *SAM2* (except *SAM2 T*) and `5 positive + negative points` for *SAM*.
- The best one-type point prompt are `5 positive points` for *SAM2* (except *SAM2 T*) and `10 positive points` for *SAM*.
- The worst performing prompt is the `centroid point`.

6.4 Preliminary guidelines for non-iterative 2D prompting

Optimizing over different objectives – such as inference time of the model, DSC as overlap metric, HD95 as surface-based metric – for different dataset characteristics leads to a high-dimensional search space. As we can already see in Fig. 6, there is no experiment with highest DSC and lowest HD95. Even for the individual datasets, only dataset D3b has a setting that maximizes both metrics: *SAM B* with `bbox+center 1C`. For the rest, a trade-off always remains on which metric to ultimately maximize. Our results can help to identify the “Pareto front” – i.e., the limit where we cannot improve one metric without decreasing the other – but deciding where to stand on that border remains application specific; highly dependent on the downstream tasks for clinical use and impact of errors. Nevertheless, based on our current results, we are already able to draw some preliminary guidelines that can help to narrow-down the optimal setting for non-interactive 2D prompting for bone segmentation in CT scans, as shown in Figure 11.

6.5 Limitations & Future Work

Our private dataset with 80 CT scans is smaller as comparable publicly available datasets (e.g., TotalSegmentator [21]). As FMs tend to leverage all publicly available datasets, performing an independent and fair comparison is increasingly challenging. We intend to keep our dataset private to prevent its use in FM training and we plan to expand it to include additional skeletal regions (e.g., hip, ankle). We believe it is essential for the research community to work collaboratively toward establishing fair and consistent benchmarks for balanced and transparent model evaluations.

Another limitation of our study is that we did not repeat experiments with varied random point positions or apply jitter to the center point or bounding box extraction which mimics human annotations more. Since prompt positioning can influence the performance, both the number and precise placement of prompt primitives play a role [1]. Since this study aims to evaluate performance under an

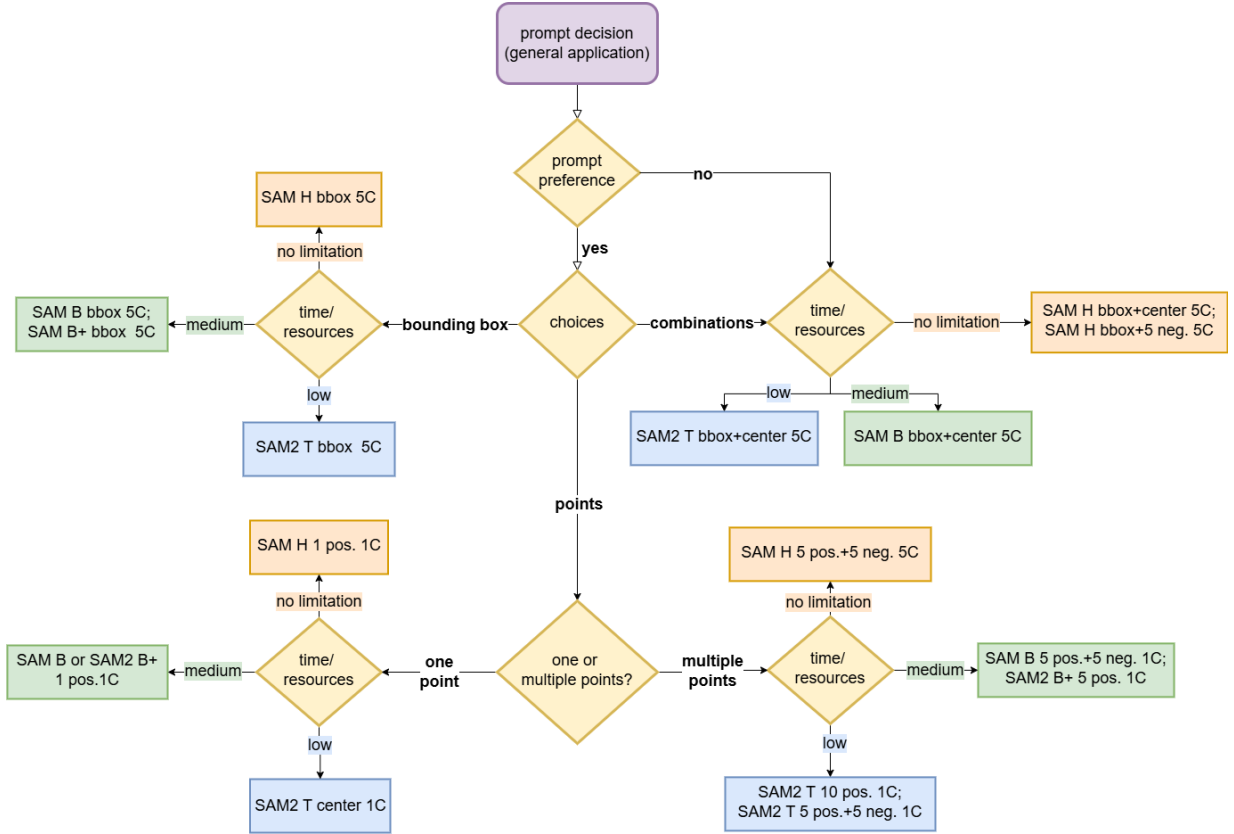


Figure 11: Preliminary guidelines for non-iterative 2D prompting based on our results.

“optimal” setting with ideal prompts (i.e., without human error or bias), we refrain from any “artificial” manipulations. However, in order to develop guidelines for robust and efficient prompting in a real-world usage scenario, additional aspects of the performance need to be considered, such as annotation time and robustness to human errors. Both are very critical factors for the performance analysis in an interactive setup with a human user. For example, we hypothesize that the annotation time for a prompt combination is longer than for a single prompt primitive and selecting multiple components (5C) takes longer than just one component (1C). Additionally, some models might be more robust to human error, e.g., when the bounding box is not a very tight enclosing rectangle. These considerations might make alternative prompt strategies more favorable considering the trade-off between segmentation performance, inference time, annotation time and robustness to human error. Future research needs to investigate human generated and interactive prompting.

A next step of our evaluation study will focus on 3D prompting for models with 3D capability, such as SAM2 [15], SAM-Med3d [20], or Med-SAM2 [27]. We anticipate more contributions from the research community in developing and fine-tuning FMs specifically for 3D medical image data after SAM2’s release. The possibilities with 3D prompting are more comprehensive, but also more complex as more components are defining for a prompt (e.g., prompt primitive, component selection, slice selection) [4]. Insights gained from this current study on 2D prompting will provide valuable guidance for informed decision-making as we design a study to test 3D models.

7 Conclusion

In this evaluation study, we evaluated four 2D SAM-family models with different model sizes for bone segmentation in CT scans. We tested 32 non-iterative prompting strategies containing one-type

(bounding box, center, centroid, positive random points), bounding box + point and point-based combination prompts. Aside from an extensive comparison of models and prompt strategies, we provide preliminary guidelines for non-iterative 2D prompting. This evaluation study is the first step towards an extensive testing of SAM-family models to be used in a clinical setting for bone segmentation in CT scans.

Acknowledgments

We thank in alphabetical order Leendert Blankevoort, George S. Buijs, Johannes G.G. Dobbe, Arthur J. Kievit, Matthias U. Schafroth, Geert J. Streekstra, Stela Topalova, Lukas P.E. Verweij, and Anemiek ter Wee for their work, support and guidance in data acquisition and curation.

References

- [1] D. Cheng, Z. Qin, Z. Jiang, S. Zhang, Q. Lao, and K. Li. Sam on medical images: A comprehensive study on three prompt modes, 2023.
- [2] J. Cheng, J. Ye, Z. Deng, J. Chen, T. Li, H. Wang, Y. Su, Z. Huang, J. Chen, L. J. H. Sun, J. He, S. Zhang, M. Zhu, and Y. Qiao. Sam-med2d, 2023.
- [3] J. Dobbe, A. Kievit, M. Schafroth, L. Blankevoort, and G. Streekstra. Evaluation of a CT-based technique to measure the transfer accuracy of a virtually planned osteotomy. *Medical Engineering & Physics*, 36(8):1081–1087, 2014.
- [4] H. Dong, H. Gu, Y. Chen, J. Yang, Y. Chen, and M. A. Mazurowski. Segment anything model 2: an application to 2d and 3d medical images, 2024.
- [5] D. Gut. X-ray images of the hip joints, July 2021.
- [6] S. He, R. Bao, J. Li, J. Stout, A. Bjornerud, P. E. Grant, and Y. Ou. Computer-vision benchmark segment-anything model (sam) in medical images: Accuracy in 12 datasets, 2023.
- [7] Y. Huang, X. Yang, L. Liu, H. Zhou, A. Chang, X. Zhou, R. Chen, J. Yu, J. Chen, C. Chen, S. Liu, H. Chi, X. Hu, K. Yue, L. Li, V. Grau, D.-P. Fan, F. Dong, and D. Ni. Segment anything model for medical images? *Medical Image Analysis*, 92:103061, 2024.
- [8] F. Isensee, P. F. Jaeger, S. A. Kohl, J. Petersen, and K. H. Maier-Hein. nnU-Net: a self-configuring method for deep learning-based biomedical image segmentation. *Nature methods*, 18(2):203–211, 2021.
- [9] J. Jia, M. Staring, and B. C. Stoel. seg-metrics: a python package to compute segmentation metrics. *medRxiv*, pages 2024–02, 2024.
- [10] A. Kirillov, E. Mintun, N. Ravi, H. Mao, C. Rolland, L. Gustafson, T. Xiao, S. Whitehead, A. C. Berg, W.-Y. Lo, P. Dollár, and R. Girshick. Segment anything, 2023.
- [11] P. Liu, H. Han, Y. Du, H. Zhu, Y. Li, F. Gu, H. Xiao, J. Li, C. Zhao, L. Xiao, X. Wu, and S. K. Zhou. Deep learning to segment pelvic bones: Large-scale ct datasets and baseline models, 2021.
- [12] J. Ma, Y. He, F. Li, L. Han, C. You, and B. Wang. Segment anything in medical images. *Nature Communications*, 15:1–9, 2024.

- [13] C. Mattjie, L. V. De Moura, R. Ravazio, L. Kupssinskü, O. Parraga, M. M. Delucis, and R. C. Barros. Zero-shot performance of the segment anything model (sam) in 2d medical imaging: A comprehensive evaluation and practical guidelines. In *2023 IEEE 23rd International Conference on Bioinformatics and Bioengineering (BIBE)*, pages 108–112, 2023.
- [14] M. A. Mazurowski, H. Dong, H. Gu, J. Yang, N. Konz, and Y. Zhang. Segment anything model for medical image analysis: An experimental study. *Medical Image Analysis*, 89:102918, 2023.
- [15] N. Ravi, V. Gabeur, Y.-T. Hu, R. Hu, C. Ryali, T. Ma, H. Khedr, R. Rädle, C. Rolland, L. Gustafson, E. Mintun, J. Pan, K. V. Alwala, N. Carion, C.-Y. Wu, R. Girshick, P. Dollár, and C. Feichtenhofer. Sam 2: Segment anything in images and videos. *arXiv preprint arXiv:2408.00714*, 2024.
- [16] S. Roy, T. Wald, G. Koehler, M. R. Rokuss, N. Disch, J. Holzschuh, D. Zimmerer, and K. H. Maier-Hein. Sam.md: Zero-shot medical image segmentation capabilities of the segment anything model, 2023.
- [17] A. Sekuboyina, M. E. Hussein, A. Bayat, M. Löffler, H. Liebl, H. Li, G. Tetteh, J. Kukačka, C. Payer, D. Štern, M. Urschler, M. Chen, D. Cheng, N. Lessmann, Y. Hu, T. Wang, D. Yang, D. Xu, F. Ambellan, T. Amiranashvili, M. Ehlke, H. Lamecker, S. Lehnert, M. Lirio, N. P. de Olaguer, H. Ramm, M. Sahu, A. Tack, S. Zachow, T. Jiang, X. Ma, C. Angerman, X. Wang, K. Brown, A. Kirszenberg, Élodie Puybareau, D. Chen, Y. Bai, B. H. Rapazzo, T. Yeah, A. Zhang, S. Xu, F. Hou, Z. He, C. Zeng, Z. Xiangshang, X. Liming, T. J. Netherton, R. P. Mumme, L. E. Court, Z. Huang, C. He, L.-W. Wang, S. H. Ling, L. D. Huynh, N. Boutry, R. Jakubicek, J. Chmelik, S. Mulay, M. Sivaprakasam, J. C. Paetzold, S. Shit, I. Ezhov, B. Wiestler, B. Glocker, A. Valentinitzsch, M. Rempfler, B. H. Menze, and J. S. Kirschke. Verse: A vertebrae labelling and segmentation benchmark for multi-detector ct images. *Medical Image Analysis*, 73:102166, 2021.
- [18] S. Sengupta, S. Chakrabarty, and R. Soni. Is sam 2 better than sam in medical image segmentation?, 2024.
- [19] Y. Shen, H. Ding, X. Shao, and M. Unberath. Performance and non-adversarial robustness of the segment anything model 2 in surgical video segmentation, 2024.
- [20] H. Wang, S. Guo, J. Ye, Z. Deng, J. Cheng, T. Li, J. Chen, Y. Su, Z. Huang, Y. Shen, B. Fu, S. Zhang, J. He, and Y. Qiao. Sam-med3d: Towards general-purpose segmentation models for volumetric medical images, 2024.
- [21] J. Wasserthal, H.-C. Breit, M. T. Meyer, M. Pradella, D. Hinck, A. W. Sauter, T. Heye, D. T. Boll, J. Cyriac, S. Yang, M. Bach, and M. Segeroth. Totalsegmentator: Robust segmentation of 104 anatomic structures in ct images. *Radiology: Artificial Intelligence*, 5(5):e230024, 2023.
- [22] J. Ye, J. Cheng, J. Chen, Z. Deng, T. Li, H. Wang, Y. Su, Z. Huang, J. Chen, L. Jiang, et al. Sa-med2d-20m dataset: Segment anything in 2d medical imaging with 20 million masks. *arXiv preprint arXiv:2311.11969*, 2023.
- [23] J. Yu, A. Wang, W. Dong, M. Xu, M. Islam, J. Wang, L. Bai, and H. Ren. Sam 2 in robotic surgery: An empirical evaluation for robustness and generalization in surgical video segmentation, 2024.
- [24] P. A. Yushkevich, J. Piven, H. Cody Hazlett, R. Gimpel Smith, S. Ho, J. C. Gee, and G. Gerig. User-guided 3D active contour segmentation of anatomical structures: Significantly improved efficiency and reliability. *Neuroimage*, 31(3):1116–1128, 2006.

- [25] Y. Zhang and Z. Shen. Unleashing the potential of sam2 for biomedical images and videos: A survey, 2024.
- [26] Y. Zhang, Z. Shen, and R. Jiao. Segment anything model for medical image segmentation: Current applications and future directions. *Computers in Biology and Medicine*, 171:108238, 2024.
- [27] J. Zhu, Y. Qi, and J. Wu. Medical sam 2: Segment medical images as video via segment anything model 2, 2024.

Appendix

A nnUNet training details

A 2D and a 3D full resolution nnUNet [8] were trained on each of the datasets individually. The default training settings have been retained, except for the data augmentation for D1 and D3 and the division into training and validation folds. For D1, the mirroring on the vertical axes is removed since bilateral scans contain right and left labels. For D3, the mirroring on the horizontal axes is removed since a horizontally flipped femoral bone and implant show some similarity with the tibial counterparts. The models for D1 and D2 are trained and evaluated on a 5-fold, for D3 on a 4-fold patient-based cross-validation split.

B Extra qualitative results

B.1 Knee dataset - cortical vs. full bone segmentation

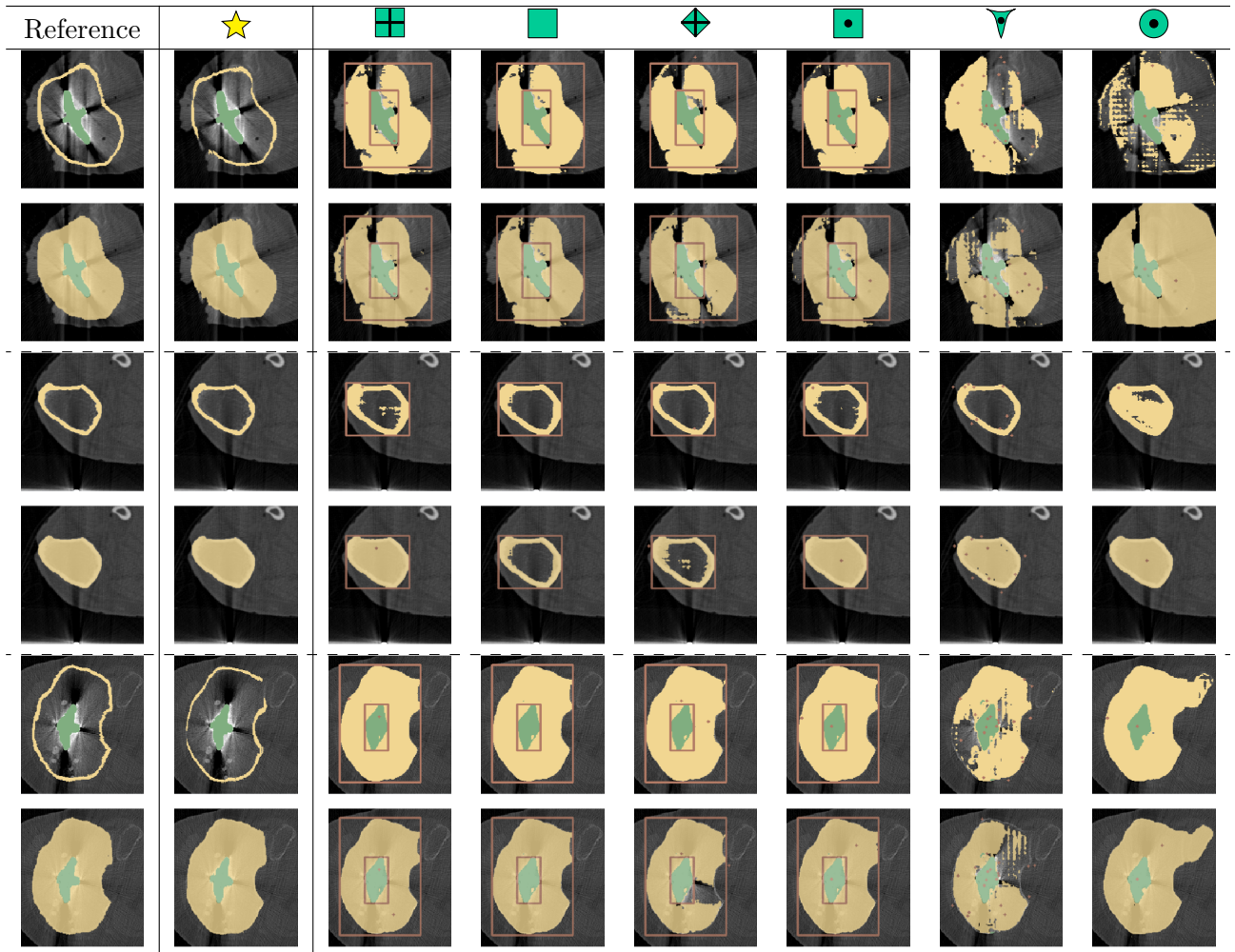


Figure 12: Examples of knee dataset in axial view for reference labels, 2D nnUNet and *SAM B* with different prompt strategies. In each row, the same axial slice is displayed with cortical (top) and full (bottom) tibia bone segmentation. The labels/prompts are color-encoded: yellow - tibia; green - tibia implant; brown - prompts for *SAM B* inference.

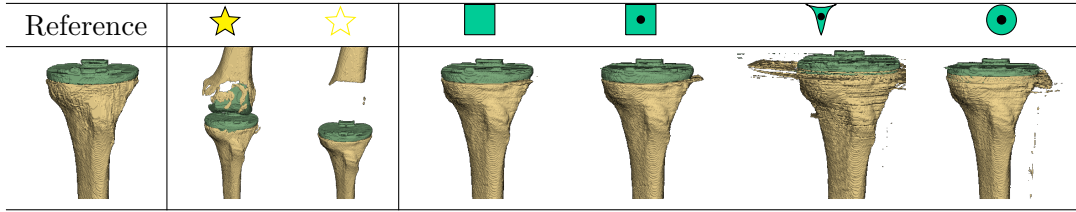


Figure 13: 3D model example for D3a for reference labels, 2D and 3D nnUNet, and *SAM B* with different prompt strategies. The labels are color-encoded: yellow - tibia; green - tibia implant.

B.2 Point-based prompting

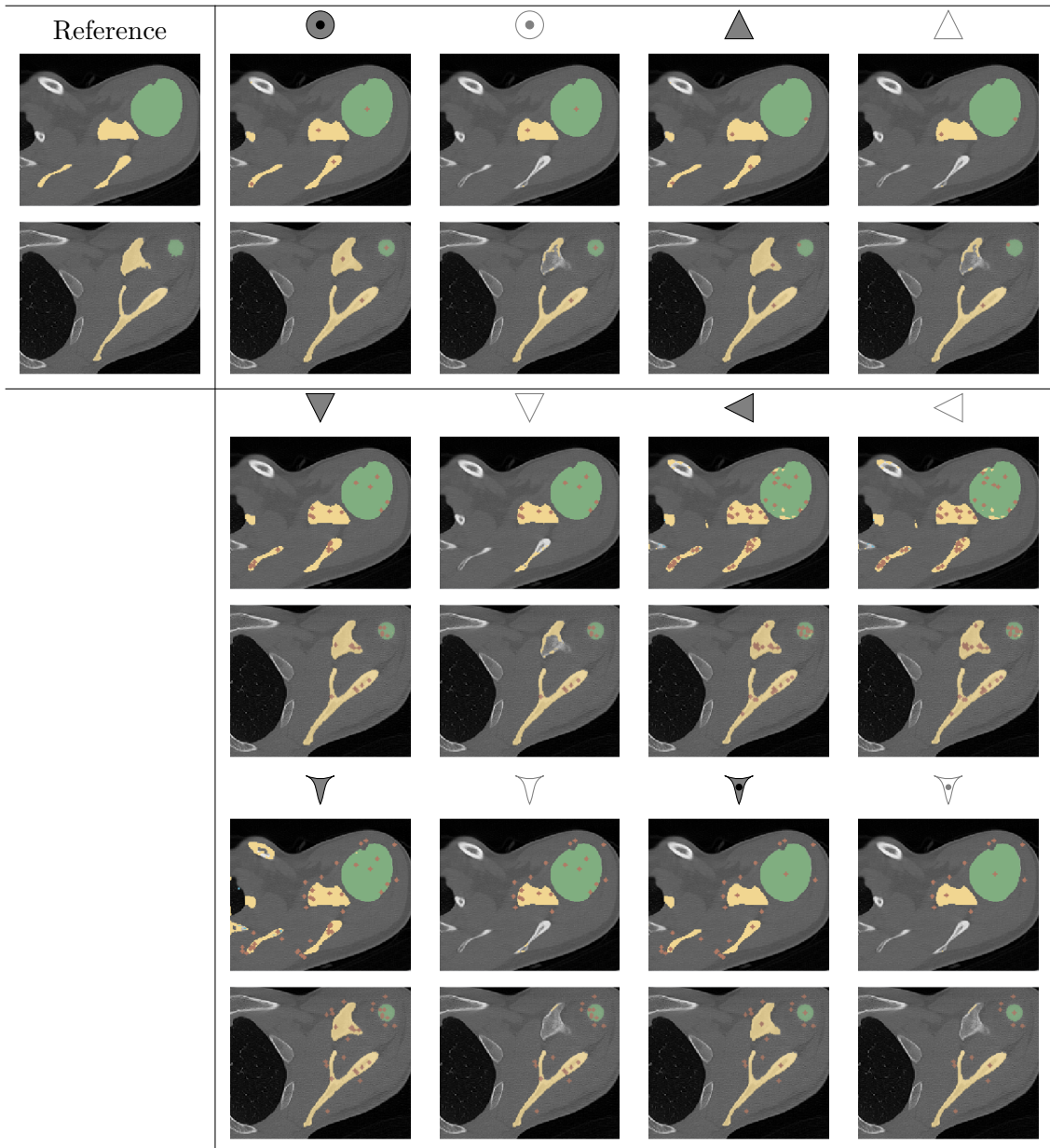


Figure 14: Examples of selected point-based strategies in axial view for reference label and *SAM B* with different point-based prompting strategies. The labels/prompts are color-encoded: yellow - scapula; green - humerus; brown - point-based prompts for *SAM B* inference.

B.3 Per Model

Selected samples of each dataset with low, medium and high associated DSC are displayed for the *Med-SAM* with bbox 1C and bbox 5C, *SAM-Med2d*, *SAM B*, *SAM L* and *SAM2 B+* and the settings bbox 5C (■), bbox+center 5C (◼) and 5 pos.+neg. 5C (▼).

Setting	DSC ↓	DSC median	DSC ↑
■			
◼			

Figure 15: Selected examples for *Med-SAM* with low, medium and high DSC.

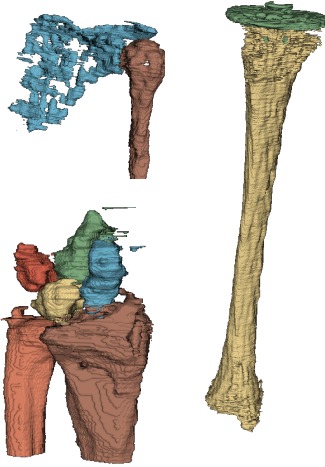
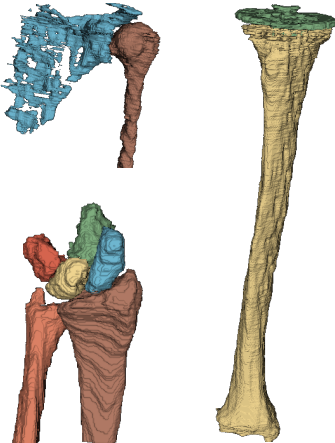
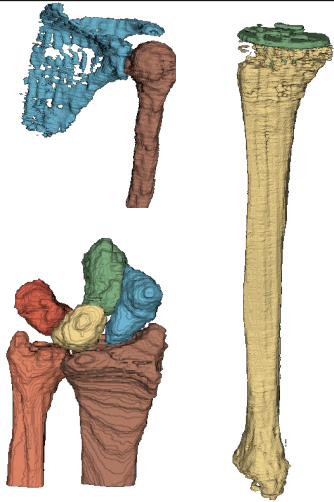
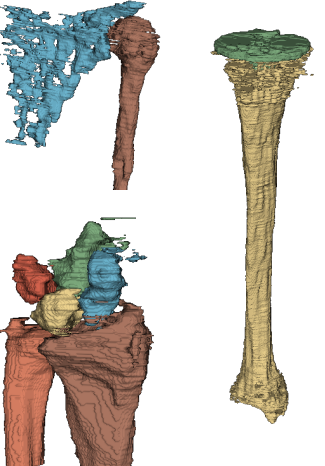
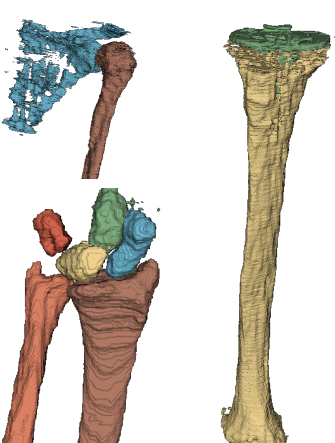
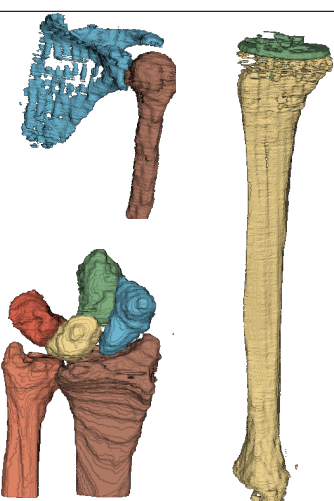
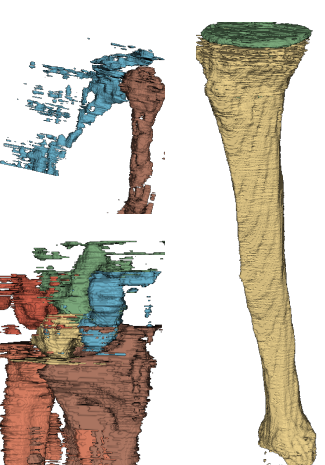
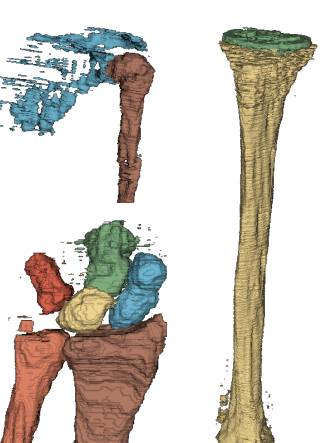
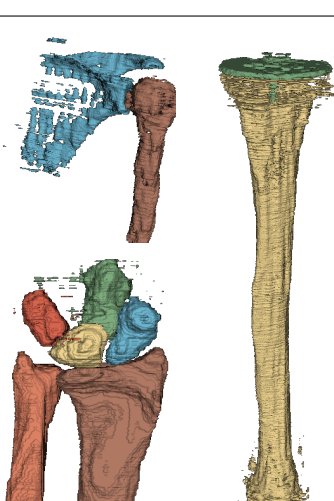
Setting	DSC ↓	DSC median	DSC ↑
			
			
			

Figure 16: Selected examples for *SAM-Med2d* with low, medium and high DSC.

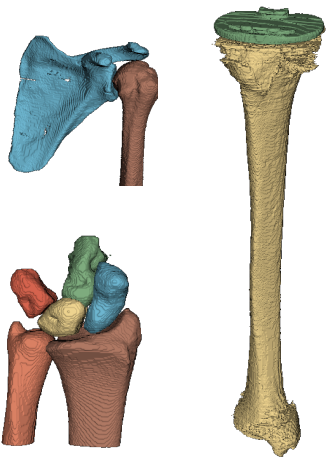
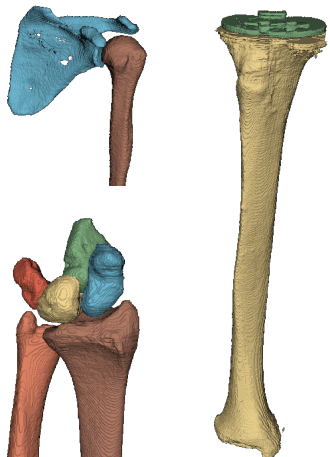
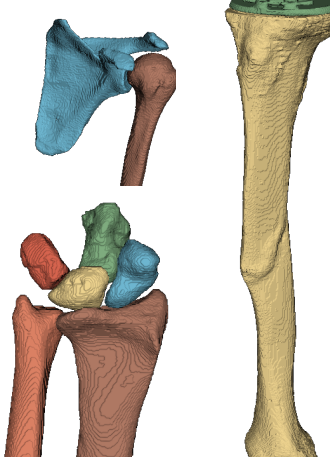
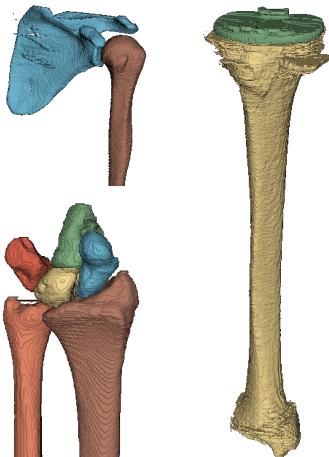
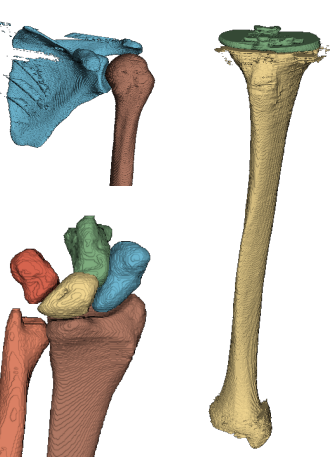
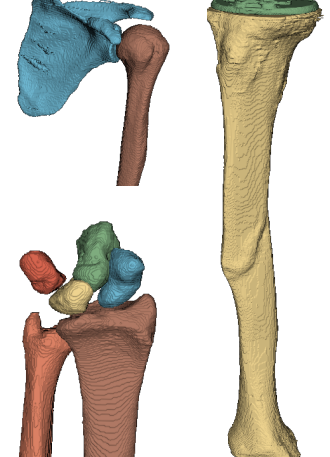
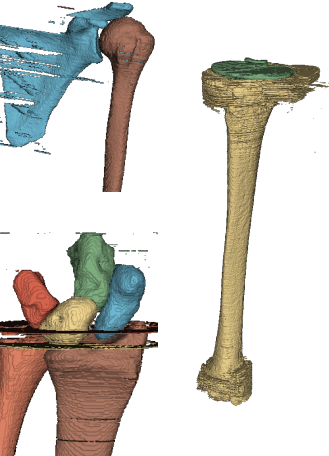
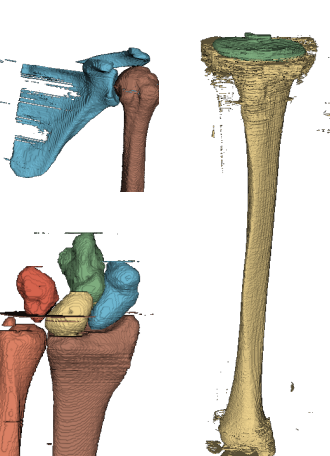
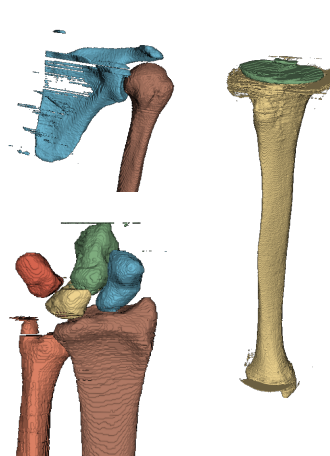
Setting	DSC ↓	DSC median	DSC ↑
			
			
			

Figure 17: Selected examples for *SAM B* with low, medium and high DSC.

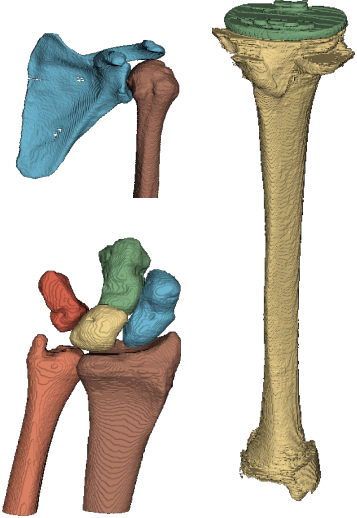
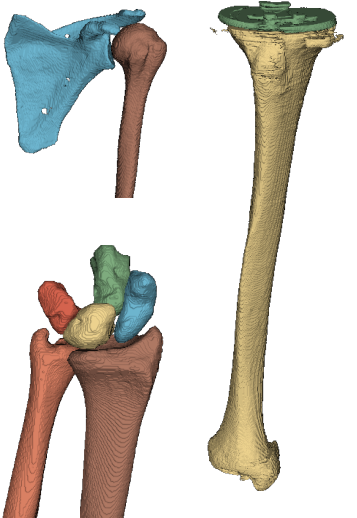
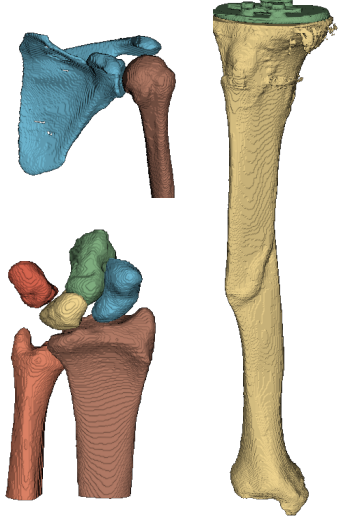
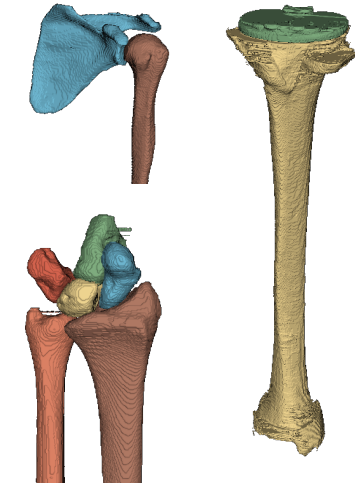
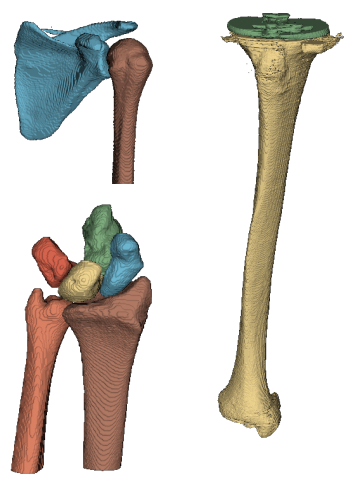
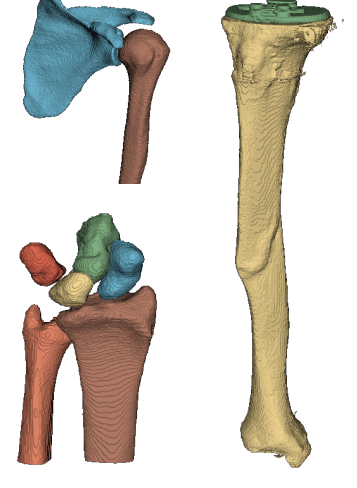
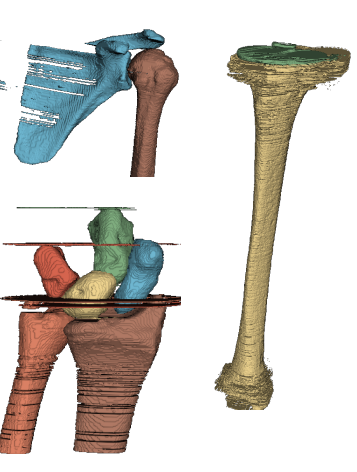
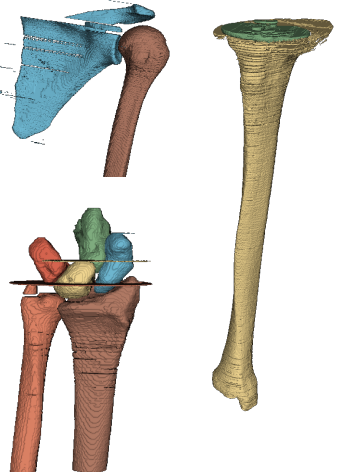
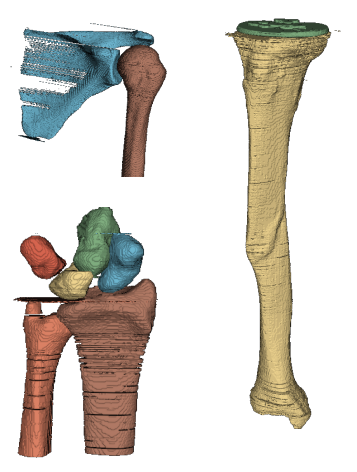
Setting	DSC ↓	DSC median	DSC ↑
			
			
			

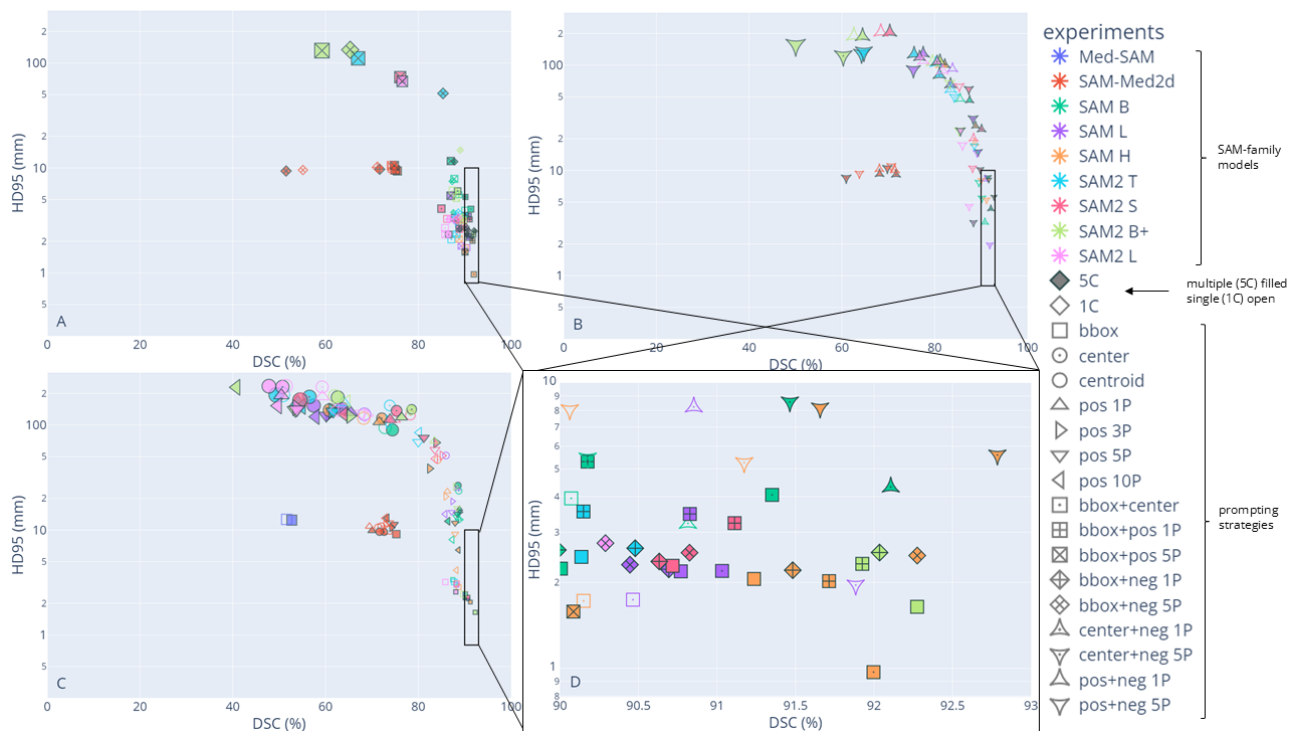
Figure 18: Selected examples for $SAM H$ with low, medium and high DSC.

Setting	DSC ↓	DSC median	DSC ↑
			
			
			

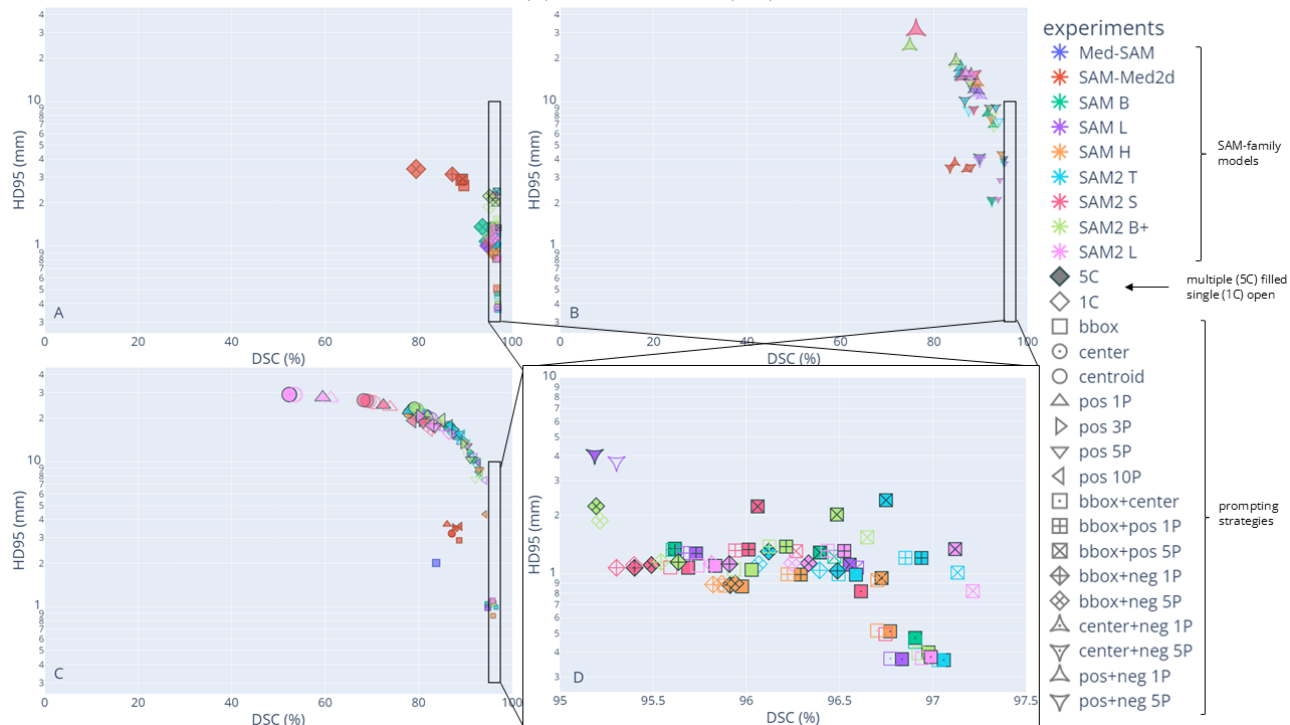
Figure 19: Selected examples for *SAM2 B+* with low, medium and high DSC.

C Segmentation performance

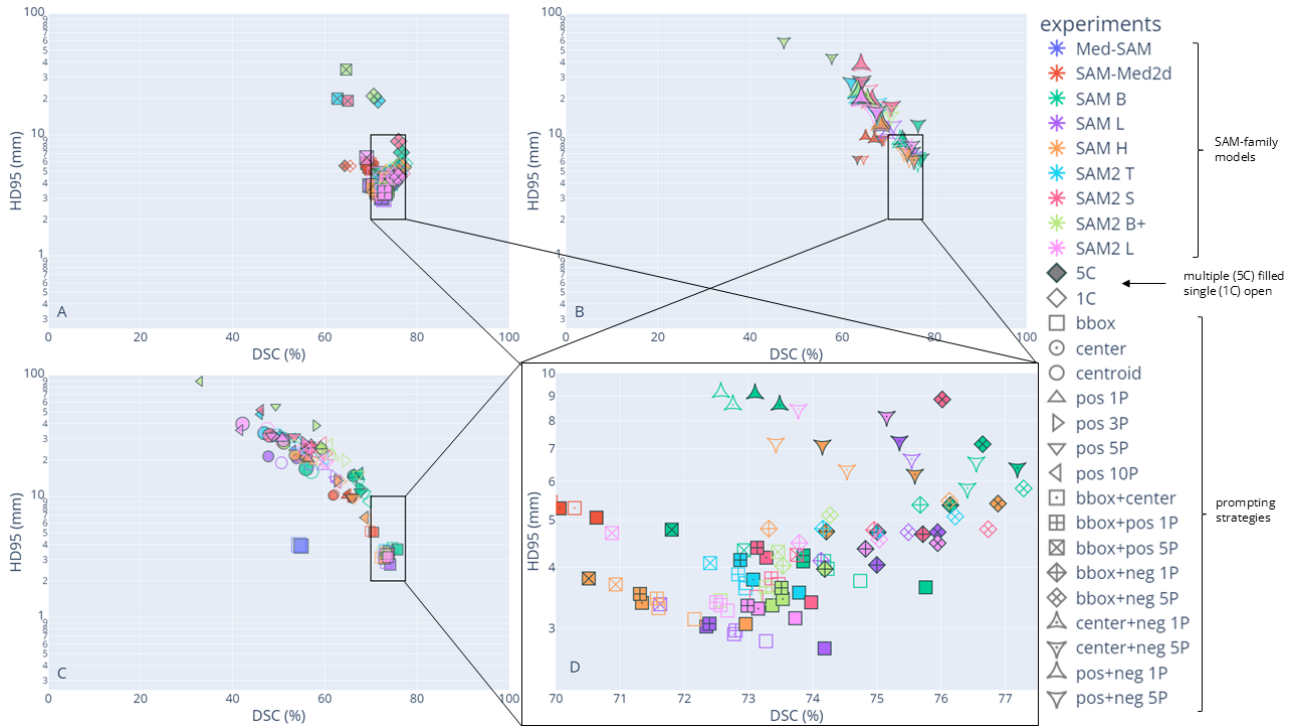
C.1 Performance for individual datasets



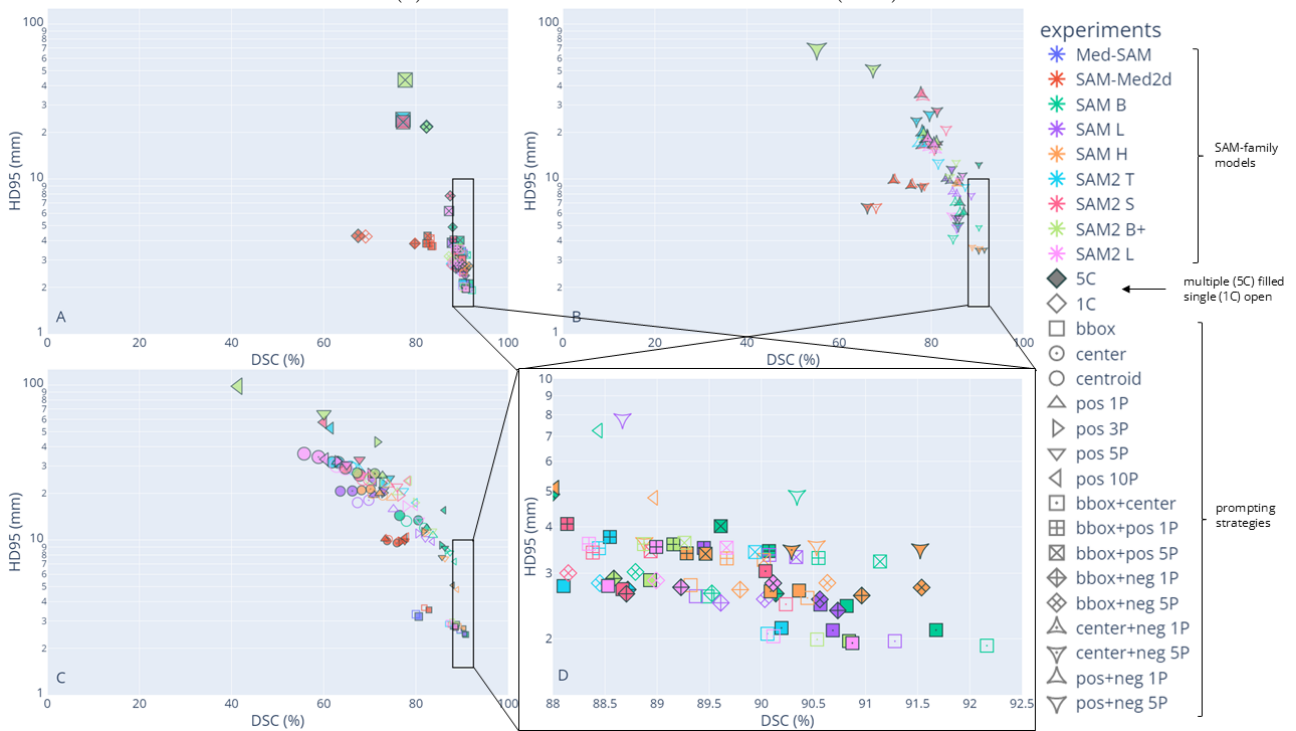
(a) Knee dataset (D1)



(b) Wrist dataset (D2)



(c) Knee dataset - cortical tibia bone (D3a)



(d) Knee dataset - full tibia bone (D3b)

Figure 20: Scatterplots for individual datasets of BPC prompts (A), PC prompts (B), OT prompts (C) and zoomed-in view to the lower right corner (D). The lower right corner, i.e., high DSC and low HD95 metrics, shows the performance strongest settings.

C.2 Performance with different number of points for individual datasets

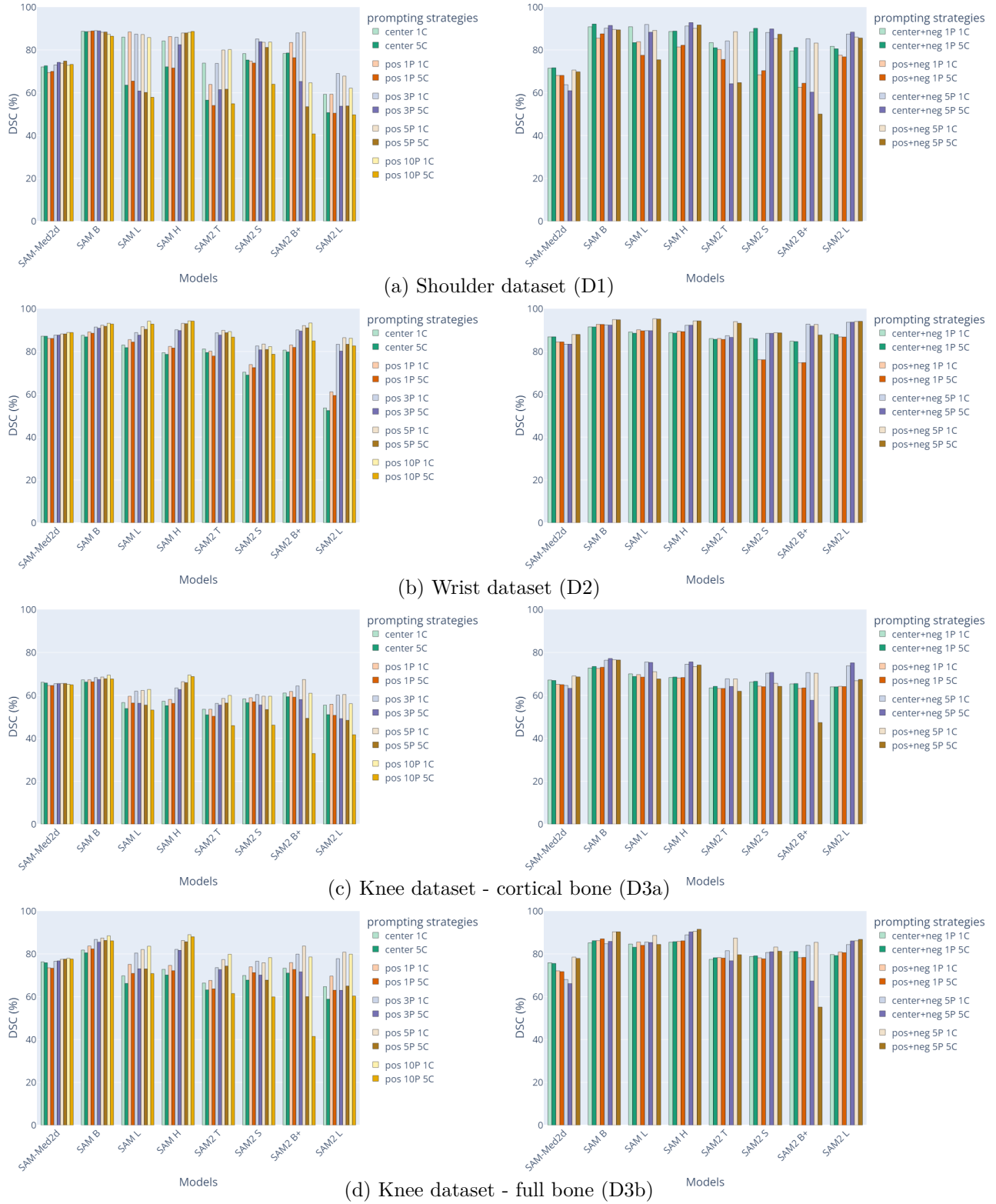


Figure 21: DSC (%) performance for different number of points per model per datasets: center point and 1,3,5,10 random positive points (left); point combinations (right).

D Performance of best performing prompts for all datasets

Table 3: Best 2D prompting strategies for individual datasets and dedicated nnUNet model as comparison (★ for 2D, ☆ for 3D full resolution). The ranking is averaged over all available models (i.e., 9 models for ■ and □; 7 models for the others) and considers the position of the prompt ranking with respect to DSC (%).

Prompt	avg Ranking	DSC (%) avg (std)	HD95 (%) avg (std)	Prompt	avg Ranking	DSC (%) avg (std)	HD95 (%) avg (std)
D1 - Shoulder dataset				D3a - Knee cortical dataset			
■	3.25	88.72 (5.7)	4.01 (3.4)	◇	4.00	74.59 (13.4)	5.13 (3.8)
■	4.00	84.58 (5.6)	4.11 (2.2)	⬠	4.62	74.32 (15.7)	4.66 (3.4)
⬠	5.88	88.24 (3.6)	3.36 (1.8)	■	5.33	71.47 (18.1)	3.53 (2.4)
■	6.75	87.22 (7.8)	4.05 (4.6)	⬠	5.88	73.64 (15.1)	4.73 (3.4)
⬠	8.38	87.19 (7.0)	4.22 (1.9)	◇	7.38	73.50 (12.7)	9.53 (10.8)
■	9.88	86.51 (8.1)	3.89 (2.8)	□	8.11	70.64 (17.3)	3.62 (2.3)
▽	11.00	85.26 (8.0)	13.85 (23.2)	■	8.25	72.65 (16.0)	3.71 (2.4)
⊗	11.75	86.41 (8.4)	4.34 (2.9)	■	8.50	72.58 (15.9)	3.81 (2.5)
□	12.00	82.33 (7.6)	4.86 (2.0)	⬠	9.38	72.56 (15.9)	3.83 (2.5)
◇	12.38	81.73 (8.7)	26.99 (27.9)	■	9.62	72.46 (15.8)	3.97 (2.6)
★	-	98.03 (1.1)	0.87 (0.2)	★	-	94.94 (3.0)	14.23 (67.0)
☆	-	98.51 (0.8)	0.91 (0.2)	☆	-	93.50 (4.5)	6.59 (22.8)
D2 - Wrist dataset				D3b - Knee full dataset			
■	1.62	95.98 (1.0)	0.74 (0.6)	■	2.00	89.81 (3.4)	2.34 (1.4)
□	2.38	95.97 (1.0)	0.70 (0.4)	■	2.62	89.72 (3.7)	2.46 (1.5)
⊗	2.50	95.81 (1.0)	1.35 (1.4)	⊗	4.38	89.06 (3.1)	3.49 (2.7)
⊗	3.75	95.69 (1.3)	1.78 (2.8)	■	5.11	87.71 (3.6)	2.83 (2.1)
■	5.00	95.30 (1.7)	1.47 (1.3)	⬠	5.38	88.35 (3.3)	2.81 (2.1)
⬠	5.75	95.24 (1.7)	1.46 (1.3)	⬠	7.12	88.37 (2.5)	3.48 (2.8)
■	7.22	93.60 (2.7)	1.33 (1.0)	■	8.00	88.24 (2.9)	3.64 (2.9)
□	8.67	93.51 (2.7)	1.34 (1.0)	⬠	9.62	87.45 (3.0)	2.90 (2.1)
⬠	10.88	94.49 (2.6)	1.31 (1.0)	□	9.78	86.62 (3.3)	2.95 (2.0)
▽	12.12	92.75 (3.8)	6.11 (8.6)	▽	10.12	86.27 (4.2)	9.70 (9.8)
★	-	98.68 (0.7)	1.05 (7.9)	★	-	96.85 (3.0)	12.51 (65.0)
☆	-	98.83 (0.4)	0.33 (0.0)	☆	-	95.82 (4.9)	4.53 (14.7)